AD-A112 317 AIR FORCE GEOPHYSICS LAB HANSCOM AFB MA F/G 1/4
RESPONSE OF CLOUD MICROPHYSICAL INSTRUMENTS TO AIRCRAFT ICING C--ETC(U)
JUL 81 M GLASS, D D GRANTHAM
UNCLASSIFIED AFGL-TR-81-0192 NL

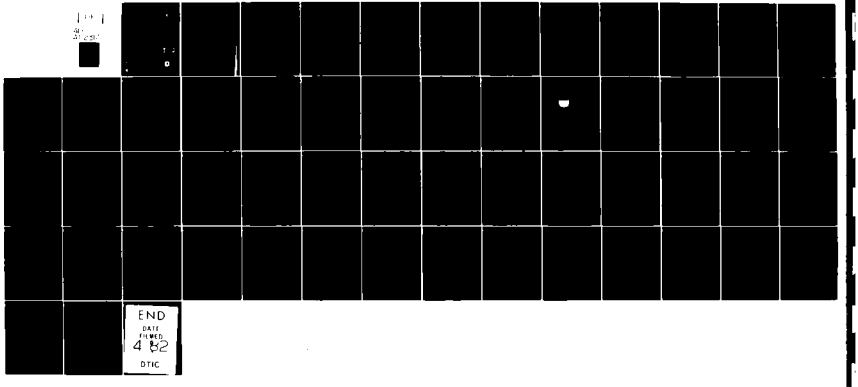

END
DATE FILMED
4 82
DTIC

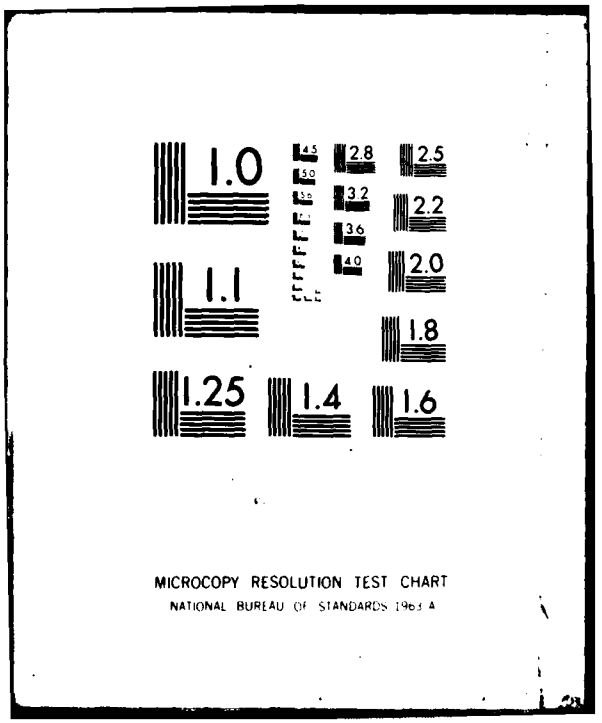
1.0
1.1
1.25
1.4
1.6
1.8
2.0
2.2
2.5
2.8
3.2
3.6
4.0
MICROCOPY RESOLUTION TEST CHART
NATIONAL BUREAU OF STANDARDS 1963 A

(12)

AFGL-TR-81-0192
ENVIRONMENTAL RESEARCH PAPERS, NO. 747

Response of Cloud Microphysical Instruments to Aircraft Icing Conditions

MORTON GLASS
DONALD D. GRANTHAM

6 July 1981

METEOROLOGY DIVISION PROJECT 6670
AIR FORCE GEOPHYSICS LABORATORY
HANSCOM AFB, MASSACHUSETTS 01731

AIR FORCE SYSTEMS COMMAND, USAF

This report has been reviewed by the ESD Public Affairs Office (PA) and is releasable to the National Technical Information Service (NTIS).

This technical report has been reviewed and is approved for publication.

FOR THE COMMANDER

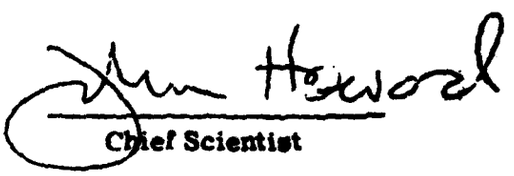

Chief Scientist

Qualified requestors may obtain additional copies from the Defense Technical Information Center. All others should apply to the National Technical Information Service.

Unclassified

SECURITY CLASSIFICATION OF THIS PAGE (When Data Entered)

REPORT DOCUMENTATION PAGE		READ INSTRUCTIONS BEFORE COMPLETING FORM
1. REPORT NUMBER AFGL-TR-81-0192	2. GOVT ACCESSION NO. AD-A112 317	3. RECIPIENT'S CATALOG NUMBER
4. TITLE (and Subtitle) RESPONSE OF CLOUD MICROPHYSICAL INSTRUMENTS TO AIRCRAFT ICING CONDITIONS		5. TYPE OF REPORT & PERIOD COVERED Scientific. Interim. 6. PERFORMING ORG. REPORT NUMBER ERP No. 747
7. AUTHOR(s) Morton Glass Donald D. Grantham		8. CONTRACT OR GRANT NUMBER(s)
9. PERFORMING ORGANIZATION NAME AND ADDRESS Air Force Geophysics Laboratory (LYC) Hanscom AFB Massachusetts 01731		10. PROGRAM ELEMENT, PROJECT, TASK AREA & WORK UNIT NUMBERS 62101F 66701006
11. CONTROLLING OFFICE NAME AND ADDRESS Air Force Geophysics Laboratory (LYC) Hanscom AFB Massachusetts 01731		12. REPORT DATE 6 July 1981 13. NUMBER OF PAGES
14. MONITORING AGENCY NAME & ADDRESS(if different from Controlling Office)		15. SECURITY CLASS. (of this report) Unclassified 15a. DECLASSIFICATION/DOWNGRADING SCHEDULE

16. DISTRIBUTION STATEMENT (of this Report)

Approved for public release; distribution unlimited.

17. DISTRIBUTION STATEMENT (of the abstract entered in Block 20, if different from Report)

18. SUPPLEMENTARY NOTES

19. KEY WORDS (Continue on reverse side if necessary and identify by block number)

Aircraft icing
Icing instrumentation
Supercooled drops
Cloud liquid water content

20. ABSTRACT (Continue on reverse side if necessary and identify by block number)

A series of passes on 6 December 1979 through multilayered-supercooled stratiform and stratocumulus clouds by the Air Force Geophysics Laboratory's instrumented C-130E cloud physics research aircraft is used to evaluate a Rosemount Ice Detector. The response of the detector to icing conditions is compared with measurements from a J-W liquid water content meter and the Knollenberg Axial Scattering Spectrometer Probe (ASSP). A procedure to adjust for zero drift of the J-W instrument is developed. Comparison of liquid water measurements from the J-W and from the ASSP indicate that these data

DD FORM 1 JAN 73 1473

Unclassified

SECURITY CLASSIFICATION OF THIS PAGE (When Data Entered)

20. (Cont)

are highly correlated and similar in magnitude. A procedure for extracting useful information from the Rosemount Ice Detector has been developed. The icing conditions in the cloud systems studied are typical of the range of conditions in winter stratiform clouds. Liquid water (LWC) values of 0.3 g m^{-3} and median volume diameters of 15 μm were most frequently observed. The results of the analysis show that the Rosemount Ice Detector is a sensitive indicator of the fluctuations of liquid water in clouds with LWC not exceeding 0.8 g m^{-3}.

Preface

The authors wish to thank Dr. Arnold A. Barnes and Ms Patricia Walsh for their careful review of the manuscript. The computer programs were written by Digital Programming Services Incorporated. Mr. Jim Lally's work with respect to this effort is particularly appreciated. Appreciation is also expressed to the following: Mr. Hugh Sweeney, for laboratory tests and calibration of the Rosemount Ice Detector; Ms Barbara Main, for preparation and improvement of the illustrations; and Mrs. Patricia Sheehy, for typing the many versions of the manuscript.

This study would not have been possible without the skillful and dedicated effort of the technical crew on the C-130E aircraft. SMSgt Tom Moraski and Sgt Wayne Domeier operated the equipment during the flight. Capt. Leandro Delgado and Mr. Don McLeod were the Mission Directors.

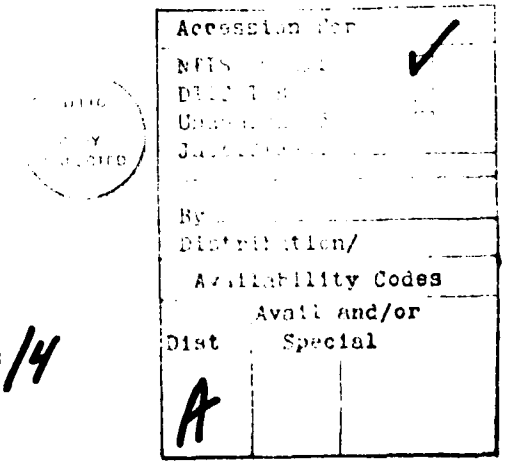

Contents

Illustrations

Tables

Response of Cloud Microphysical Instruments to Aircraft Icing Conditions

1. INTRODUCTION

In recent years, there has been renewed interest in the problem of aircraft icing. This has come about as a result of the great expansion of the private and business aircraft industry, the great increase in the military and civilian use of helicopters, and the requirement for high-performance military aircraft operation in potential icing environments.

The Air Force, for example, has turned to low-level operations as a means of increasing the survivability of its aircraft. This is caused in part by the sophisticated mid- and low-level air defense equipment now generally available. A return to low levels brings us back to a region of the atmosphere not frequently traversed by the United States Air Force since the advent of the high performance jet engine. This step "back" has caused the re-emergence of the 30-year old problem of aircraft icing. Faced with this problem, we find that our responses are based on technology developed during the 1950's.

The renewed interest in airframe icing may be surprising, but it probably should have been expected. Experience with safety and operating problems research has shown that such problems are "solved" for a time, and then as aircraft designs and operating practices change, these problems return and call for renewed effort, often in terms of a finer-scale solution than offered earlier. New aerodynamic

(Received for publication 19 June 1981)

designs have emerged which raise questions of icing vulnerability for which existing data are inadequate. Expanded operational regimes for both civil and military rotorcraft, as well as general aviation aircraft, have greatly increased the exposure of these classes of aircraft to icing threats.

Recent symposia (for example, AGARD report,[1] Frost and Camp,[2] and Blaha[3]) have outlined new problems associated with modern aircraft and helicopters, described new research and data gathering programs, and encouraged a re-examination of considerable work done by the National Advisory Committee for Aeronautics (NACA) and others on this subject during the 1940's and 1950's.

The range of values of the basic meteorological parameters associated with icing was summarized by Perkins.[4]

Temperature	down to	-35°C
Liquid water content	to	1.5 g/m^3
Droplet size	5 μm to	50 μm
Maximum distance of icing conditions		350 km

The formation of ice on aircraft surfaces, as well as the rate at which it accretes, is not solely dependent on atmospheric conditions but also on aircraft factors such as speed, aerodynamic shape and dimension. The meteorological and aircraft components to the problem of aircraft icing have been discussed by Lewis.[5] The nonmeteorological parameters interact with the ambient environment in a complex manner; for example, at a given ambient temperature dynamic heating effects due to aircraft speed and aerodynamic shape could cause ice that is formed either to melt or become more dense. The aircraft characteristics also determine the collection efficiency with respect to droplet size and thus the mass of ice collected. The response of each aircraft type to icing conditions is therefore a separate issue. Studies by Jackson,[6] and Hankey and Kirchner[7] are two recent examples of icing research primarily concerned with aircraft aerodynamic characteristics.

In this report, we are concerned only with the meteorological parameters associated with aircraft icing. The purpose of this report is to describe the analysis technique developed and to evaluate an ice detector recently installed on the Air Force Geophysics Laboratory instrumented Cloud Physics Research MC-130E aircraft. Its response will be related to the response of independent measures of liquid water content (LWC) over the range of conditions observed. In the course of

(Due to the large number of references cited above, they will not be listed here. See References, page 49.)

this description, the microphysical characteristics of a cloud system in which a range of icing conditions was observed will be described.

As part of the Aircraft Icing Probability Program of the Meteorology Division, the data selected for use in this study are from one of a series of flights made to investigate the meteorological conditions associated with aircraft icing.

2. METEOROLOGICAL SITUATION

The AFGL meteorologically-instrumented MC-130E was flown on a racetrack course in the vicinity of Huntington, West Virginia from approximately 2300Z, 6 December 1979 to 0100Z, 7 December 1979. Figure 1 shows the time-height profile of the flight. Twelve data gathering passes (legs) were made at approximately 0.6-km (2 kft) height intervals. Level-flight passes were made at odd thousand-foot altitudes on the ascending portion of the flight and at even thousand-foot altitude intervals on the descent.

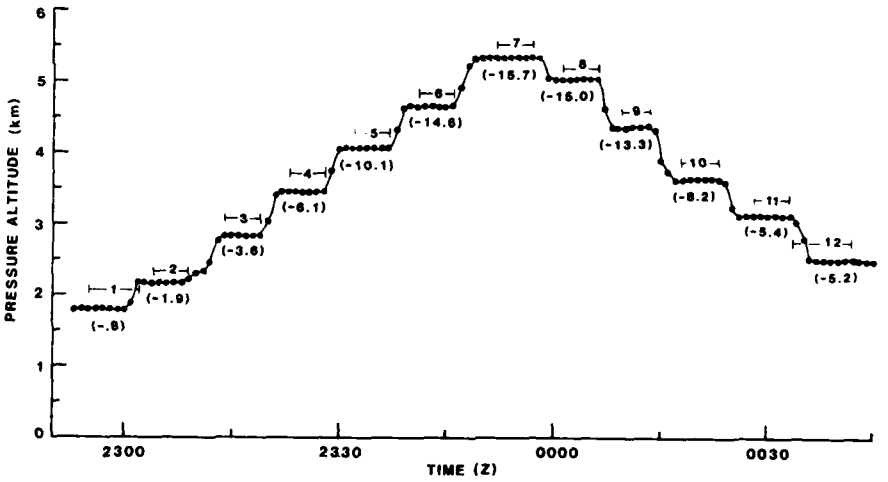

Figure 1. Flight Profile of Icing Study Mission on 6 December 1979 (Flight No. 79-47). Pass numbers and mean temperatures (in degrees Celsius) for each pass are indicated

The flight time as well as location, was made to coincide with the release of the 0000Z, 7 December 1979 rawinsonde from the National Weather Service station at Huntington, West Virginia. Figure 2 shows the skew-T plot of temperature and

dew-point profile from that rawinsonde observation. The aircraft flight was made in a moist layer extending from about 1- to 5-km altitude on the lee side of a long wave trough just behind a well-defined surface cold front. The data gathering legs commenced at about 1.8 km, in the frontal inversion just above the freezing level. In this region, multiple layers of broken to overcast clouds were observed, the source of the data analyzed in this study.

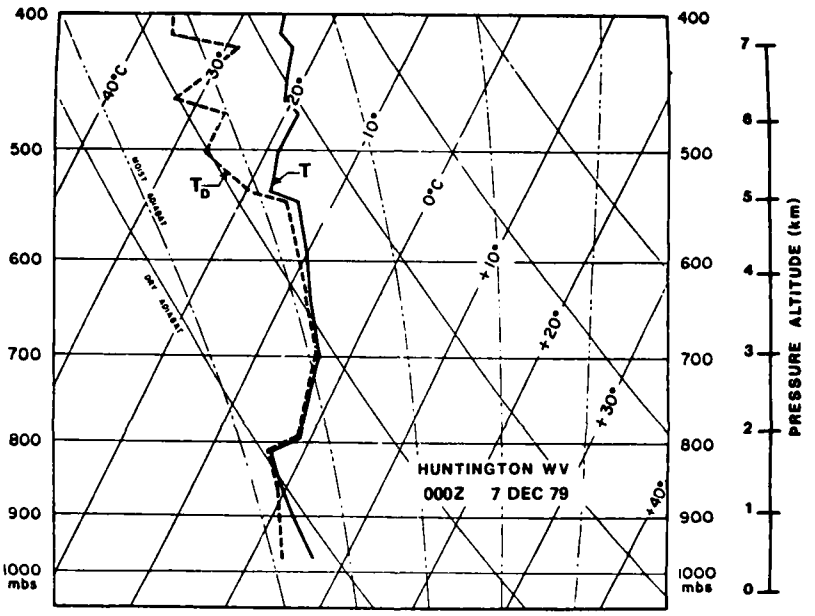

Figure 2. Temperature, T, and Dewpoint, T_D, Profile From Huntington, West Virginia, 0000Z, 7 December 1979 Radiosonde

The 0000Z, 7 December 1979 synoptic weather charts are presented in Appendix A. The charts for surface pressure, 700-mb heights and isotachs, and 700-mb temperature and dew-point depression are shown in Figures A1, A2, and A3, respectively. In each chart, the aircraft flight region is shown in the cross-hatched area centered on Huntington, West Virginia. The surface pressure chart shows that about 100 km east of the flight zone an active, eastward moving cold front, paralleling the Allegheny Mountains, extended from northern New York southwestward into the Gulf of Mexico. A band of precipitation, consisting generally of steady light rain extended westward from the frontal zone for 150 to 200 km and encompassed

the flight area. In this region, there were multiple layers of scattered to broken stratocumulus between 600 and 1200 m, with higher layers of broken to overcast mixed altostratus and altocumulus between 2 and 5 km. Immediately behind this band of light precipitation and clouds, a strong ridge from the southwestern states produced a rapidly clearing region.

The 700-mb charts (about 3 km altitude) indicate that the flight zone was on the leeward side of a broad, longwave trough containing a tongue of moist air that extended from slightly below the 850-mb level to just above the 700-mb level. The atmosphere above the maximum flight level was found to be a region of weak subsidence. This was evident from analysis of 500-mb data. [Note the skew-T plot (Figure 2).]

3. STANDARD INSTRUMENTATION

The principal instruments used to characterize the meteorological conditions associated with icing are the following: The Rosemount Total Temperature Probe for obtaining true air temperature; the Johnson-Williams Hot Wire Liquid Water Content Meter for determining LWC from droplets of diameter ≤ 30 μm; and the Particle Measuring System's Axially Scattering Spectrometer Probe (ASSP) for obtaining droplet number concentration, LWC and median volume diameter. These instruments, together with the recently installed Rosemount Icing Rate Meter, are described in this and following sections along with the procedures developed to obtain usable information for them. A list of the cloud physics instrumentation carried on board the MC-130E aircraft and a diagram showing location of the probes, are included in the Appendix (Figure A4).

3.1 Total Temperature Probe

Temperature information is obtained with the use of a Rosemount Temperature Probe. The principle of operation is the known relation of temperature to resistance of a platinum wire element, the exposed component of the probe's bridge circuit. The probe measures total temperature, (T_{TOT}); that is, the true temperature (T) of the air* plus a temperature contribution due to dynamic heating which varies with the Mach number, M. These are related according to the expression

$$T_{TOT} = T (1 + k M^2) \qquad (1)$$

*The probe is subject to a small error due to possible wetting by cloud droplet. This results in cloud temperatures appearing slightly colder than they actually are.

where

$k \approx 0.1992$ a ventilation factor

and

$$M = [5((\Delta P/P+1)^{0.286} - 1)]^{1/2}.$$

The Mach number, M, is a function of ambient pressure (P) and dynamic pressure excess (ΔP) due to the aircraft's speed. During this study, all data were collected while the aircraft flew at ~150 knots indicated air speed (IAS) ($\Delta P \sim 37$ mb). The true air speed (TAS), calculated from the relation

$$TAS = B(T)^{1/2}M, \text{ where } B = 20.05 \text{ m sec}^{-1} \text{ deg}^{-1} \quad (2)$$

was found to vary from ~88 m/sec at the lowest pass altitude to ~95 m/sec at the highest.

3.2 Johnson-Williams Liquid Water Content Meter

The Johnson-Williams (J-W) instrument has been the most widely used device for the measurement of cloud LWC. It operates on the principle that a heated resistance wire mounted perpendicular to the airstream will decrease its resistance in proportion to the extent to which it is cooled when a droplet strikes it and evaporates, the amount of cooling being related to droplet mass.

The probe was originally used and calibrated by Neel and Steinmetz[8] and Neel[9] in their studies of aircraft icing. Further calibration work by Owens[10] and comparison with other devices (Spyers-Duran,[11] Knollenberg[12]) have shown the probe to be a sensitive and adequate measure of LWC when particle diameters are ≤ 30 μm; that is, small cloud droplets. The model mounted on the MC-130E aircraft has a second resistance wire mounted parallel to the airstream, connected as an adjacent leg of the bridge circuit. It is assumed that this element is not subject to water drop impingement. Its purpose is to compensate for effects due to variations in airspeed, altitude, and temperature so that the output of the probe bridge remains proportional to the rate of mass impinging on the sensing wire. Changes in angle-of-attack and yawing of the aircraft affect the instrument's means of compensating correctly for these extraneous effects. This results in a tendency for the instrument zero position to drift.

(Due to the large number of references cited above, they will not be listed here. See References, page 49.)

Figure 3 is a scatter plot of the LWC from the J-W with height for each second during the icing studies flight on 6 December 1979. The adjustment procedure for these data assumes that during a pass at each of the flight levels there exists a time when the LWC ≈ 0.0 g m^{-3}. This assumption implies that continuous unbroken clouds are not observed. The minimum values observed are then an indication of the extent of the instrument drift. Thus an adjustment for each point can be obtained.

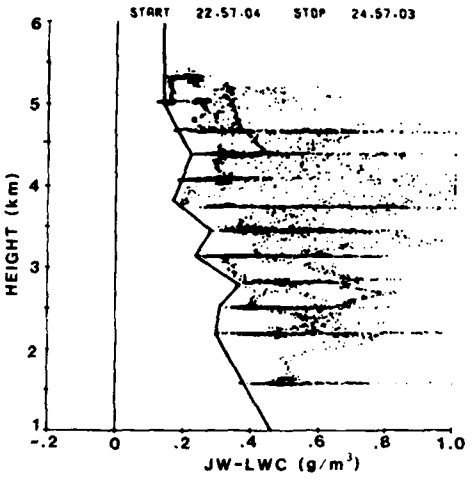

Figure 3. Scatter Plot of Unprocessed J-W Data for Each Second of Flight on 6 December 1979. Flight No. 79-49. Line segments shown are used to adjust data. Coordinates and slope of each line segment are given in Table 1

The method developed does not attempt to isolate and compensate for each of the assumed causes of drift, but it adjusts the data for their combined effect by a set of reference linear equations connecting the well-defined minimum positions. The values observed, $(LWC(JW)_{OBS})$, at each second, and at height, H_{OBS}, are corrected according to the equation:

$$LWC(JW) = LWC(JW)_{OBS} - \left\{ LWC_I + \frac{LWC_I - LWC_{I-1}}{H_{I-1} - H_I} (H_I - H_{OBS}) \right\} \quad (3)$$

where I and (I-1) refer to adjustment values defined at the upper and lower bounds, respectively, of each line segment. Table 1 lists the correction parameters obtained for data collected on this flight. The revised scatter plot of all LWC values due to these corrections are shown in Figure 4.

Table 1. Correction Parameters Applied in Eq. (3) to Obtain Adjusted Values

H_I(km)	LWC_I(g/m^3)	ΔLWC/Δ H
6.00	0.136	0.0
5.00	0.136	0.115
4.40	0.205	-0.054
3.80	0.173	0.321
3.45	0.285	-0.204
3.14	0.222	0.516
2.83	0.382	-0.193
2.44	0.307	-0.055
2.20	0.293	0.114
1.0	0.430	-----

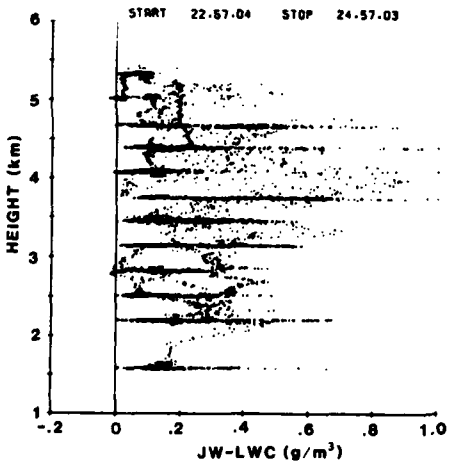

Figure 4. Scatter Plot of J-W Data After Corrections Described in Text (negative values set = 0)

3.3 Axial Scattering Spectrometer Probe

The Axial Scattering Spectrometer Probe (ASSP) manufactured by Particle Measuring Systems (PMS) Incorporated, sizes particles by measuring the amount of light a particle scatters as it passes through a He-Ne laser beam. The amount of scattered light is related to particle size. In the system installed on the MC-130E aircraft, particles are sized and counted in 15 equally spaced size classes (binwidth = 2.0 μm) whose nominal range is 2 to 30 μm. The characteristics of

this instrument and its limitations with respect to size resolution were discussed by Pinnick and Auverman,[13] and by Walsh.[14]

The instrument was calibrated by the PMS some months following its use in the data collection program. The output of the laser was found to be only 60 percent of its normal intensity owing to decay. This resulted in a droplet size classification too low by a factor of 1.4. Thus the channel containing 10-μm diam droplets with normal laser intensity, under these conditions would contain 14-μm droplets. For this case, the binwidth is 2.8 μm.

A study was made for comparison of the results obtained by calculating liquid water content, from data collected during the 6 December 1979 flight, using the following assumptions: (1) The laser had not decayed; (2) the laser had decayed to 60 percent of normal; and (3) that at the time these data were collected, decay of the laser had progressed only to the point where droplets were being classified too low by a factor of 1.2. Each of the 15 channels was therefore assigned for this latter case a binwidth of 2.4 μm. The droplet diameters assigned to each channel for the three conditions being compared are listed in Table 2.

Table 2. Droplet Diameters Assigned to Each Channel for Indicated Binwidth

Binwidth Channel	Nominal 2.0 μm	Calibrated 2.8 μm	Assumed 2.4 μm
1	2	2.8	2.4
2	4	5.6	4.8
3	6	8.4	7.2
4	8	11.2	9.6
5	10	14.0	12.0
6	12	16.8	14.4
7	14	19.6	16.8
8	16	22.4	19.2
9	18	25.2	21.6
10	20	28.0	24.0
11	22	30.8	26.4
12	24	33.6	28.8
13	26	36.4	31.2
14	28	39.2	33.6
15	30	42.0	36.0

13. Pinnick, R.G., and Auverman, H.J. (1979) Response characteristics of Knollenberg light-scattering aerosol counters, J. Aerosol. Sci. 10:55-74.

14. Walsh, P.A. (1977) Cloud Droplet Measurements in Wintertime Clouds, M.S. Thesis, Univ. of Wyoming.

The effect these differences in diameter have on LWC calculations are evident from the formula:

$$LWC = \frac{\pi}{6} \rho \sum_{i=1}^{15} N_i D_i^3 \qquad (4)$$

where

ρ = water density
N_i = number of droplets in channel i per m^3
D_i = adjusted diameter of droplet in channel i

Some examples indicating the differences in LWC profiles due to use of the three binwidths are shown in Figure 5(a, b, c). These illustrate the sensitivity of the liquid water mass calculations to proper diameter calibration.

4. COMPARISON OF THE AXIAL SCATTERING SPECTROMETER PROBE AND THE JOHNSON-WILLIAMS INSTRUMENT

The close agreement both in magnitude and shape of the Axial Scattering Spectrometer Probe (ASSP) curves adjusted to binwidths of 2.4 μm with the Johnson-Williams (J-W) derived data suggests that this choice of binwidth is reasonable for use throughout the study in the calculation of LWC, and that both the J-W and ASSP are responding similarly to the cloud spectrum. This result is in agreement with Knollenberg's[12] conclusion. In a later section, further evidence of the similarity of response of the two instruments will be seen in the LWC plots with time (Figure 9) during selected passes. As will be seen in Figure 9(c), and as evident in Figure 5(c), some residual zero drift error can remain in the adjusted J-W values of liquid water. This is because the correction procedure allows some subjective latitude in determing correction coefficients. However, in this study, these small drift errors were allowed with further corrections.

Since the J-W does not respond to frozen particles, significant differences in the shape of the two measures of LWC with time would indicate that the cloud contains both supercooled and frozen particles in this size range. This is tested by correlating data sets from each of 68 icing events (that is, cycles of the ice detector). A large percentage of these cases was highly correlated (see Figure 6).

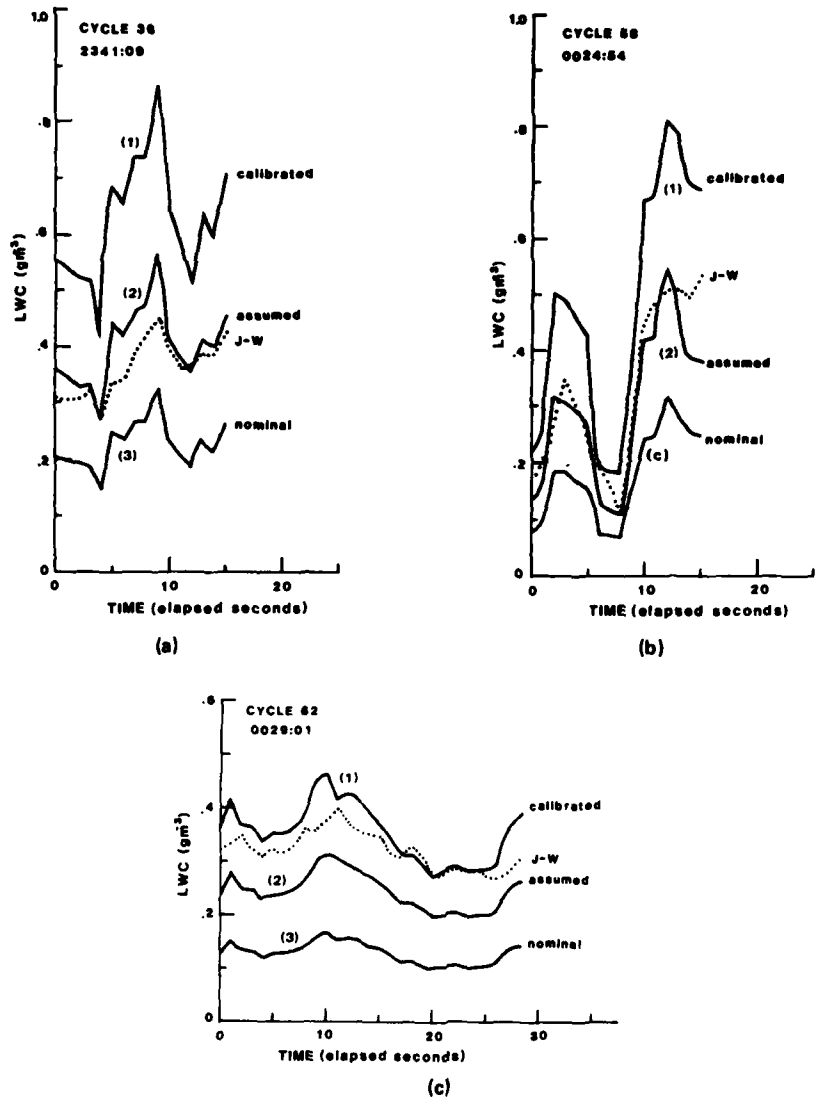

Figure 5. Three Examples of LWC From ASSP Using (1) Calibrated, (2) Assumed, and (3) Nominal Binwidth. J-W derived LWC shown for comparison

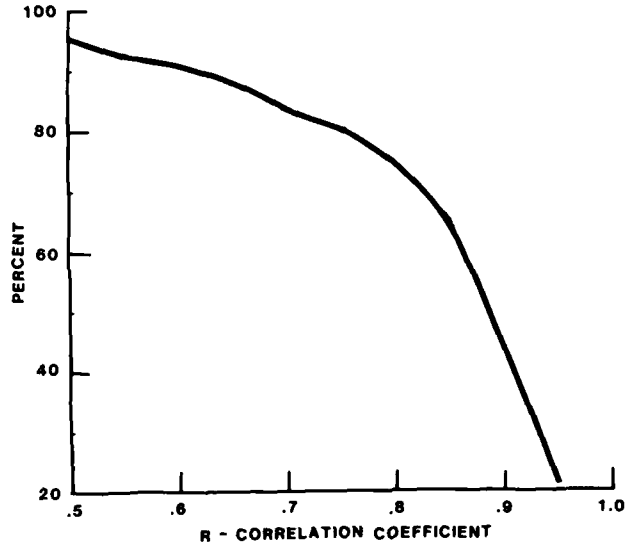

Figure 6. Percentage of Cases Where Correlation of J-W and ASSP Data Exceeded Value Shown

An over-all comparison of the response of the J-W and ASSP was made after adjusting these data as previously described. A least-squares fit using data from each second of the 2-hour flight gave the relation:

$$LWC_{J-W} = 0.081 + 0.822\ (LWC_{ASSP}) \tag{5}$$

with RMS error of 0.079. The over-all correlation coefficient was 0.86.

The PMS 1-D cloud probe which counts particles in the 20 to 300 μm size range was also operated during the data collection program. Data collected during this flight indicate that the liquid water contribution from the cloud probe to the total water measured was, except for a few minutes of the flight, one to two orders of magnitude less than that contributed by the axial probe. Therefore it is reasonable to conclude that both the J-W and axial probe responded to the predominant droplet population characterizing the cloud system and both adequately estimated the liquid water content associated with icing conditions. During the flight, some snow was observed during the first three passes (made at the lowest levels). The difference in total LWC (that is, sum of LWC from axial and cloud probes) from that measured by the ASSP alone is probably due to frozen particles (see Table 4).

In a later section describing the response of the Rosemount Ice Detector, only data from the PMS probes will be used for comparison. With the PMS probes,

droplet spectra information is available and the median volume diameter (MVD), a useful parameter for describing icing conditions, can be calculated. Median volume diameter is defined as the diameter, over the size range considered, where one half the total mass is contained in the droplets smaller (greater) than it.

5. THE ROSEMOUNT ICE DETECTOR

The Rosemount Ice Detector, Model 871FA (Figure 7) is installed at the undersurface and near the center of the right wingtip of the aircraft. The sensing element (probe) of the detector is a cylindrical tube 0.635 cm in diameter and 2.54 cm in length mounted on a 5-cm airfoil strut extending into the free airstream. These external elements are attached to the detector's control circuitry housed in a mounting that protrudes 2.5 cm from the wingtip undersurface. The probe tip is then 10.2 cm below the wing surface. It is vibrated longitudinally by a magnetostrictive oscillator at a resonant frequency of 40 kHz when dry. With accumulation of ice on the probe, the resonant frequency decreases. The decrease in vibration frequency is proportional to mass accumulated and, as related by the manufacturer, to a thickness of ice on the probe. There is no reason, however, to assume or to require that the mass accumulates uniformly along the probe length.

To derive information from this instrument, a procedure for data reduction was developed based on its operational modes, its response as determined from laboratory calibration, and the nature of the recorded data with the aircraft in icing situations.

The operational modes of the Rosemount Ice Detector are: (1) Sensing; (2) Detecting; and (3) Standby. These modes, as described here, operate in the order given. Together the three comprise one cycle of the instrument.

When the detector is in the sensing mode, the probe signals that ice is accumulating on it. The change in oscillating frequency due to mass accumulation is converted by the Rosemount Ice Detector to a dc voltage. The voltage is processed along with all other meteorological information through voltage conversion oscillators (VCO's) to digital form and recorded each second. These processed values have a possible range of 0-9999 counts and are directly analogous to probe output volts. In this mode, the counts range from approximately 6250, indicating no ice condition to 9818, the trip point for heating of the probe. The latter value as determined by laboratory tests, is the point at which sufficient mass has been accumulated on this probe to trigger the detecting mode. It is possible for the probe to remain in the sensing mode when icing rates are low and evaporation prevents buildup of mass. With evaporation of ice the counts decay to approximately 6250.

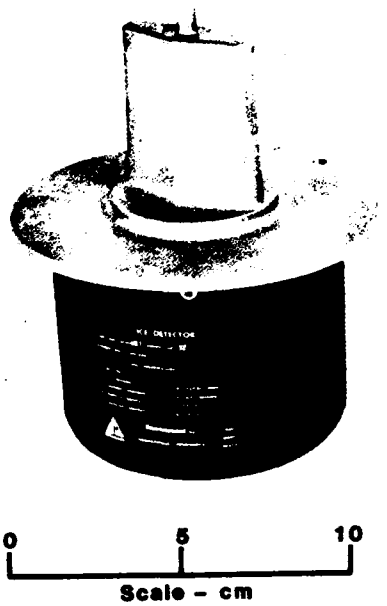

Figure 7. Rosemount Ice Detector Model 871FA. The unit is mounted on the undersurface of the right wingtip of the aircraft

In the detecting* mode an icing signal is generated and the probe heated in order to melt off accumulated ice. The heating period lasts 5 ± 2 seconds. During this period, random counts are generated and values ranging from 0 to 9999 counts may be observed. These values are neglected as data, but used as an indicator of a change from the detecting to the standby mode.

The standby mode occurs when both heater current and signal reference voltage are inactivated. All ice has been removed from the detector. The counts in this mode range narrowly about 5250.

The time needed for the ice detector to return from the standby to the sensing mode (~6250 counts) is the time required for the probe to cool to ambient temperature. (The fact that the counts return to ~6250 when going from standby to sensing verifies that no ice remains on the probe.) The time required to cool depends on icing conditions, ambient temperature and the aircraft's true airspeed. In cases of moderate icing, 7 to 10 sec are typical.

*The instrument was originally designed to "detect" the presence of icing and to turn on a warning light/buzzer in the cockpit along with activating the probe heaters. Hence the heating portion of the instrument cycle was designated by the manufacturer as the detecting mode.

In the analysis procedure developed, the sensing mode is defined as beginning 7 sec after counts exceed 6000 and ending when counts reach 9818. The time included by these limiting values provides a working definition of the icing period. However, for heavy icing conditions, the cycling of the ice detector is so rapid that this working definition breaks down. A modification of this definition is described in the analysis section.

In addition, an interpolation scheme is applied to the counts during data reduction to remove occasional large excursions, that is, spike values exceeding 400 counts (< 6 during this flight) lasting only 1 to 2 sec and observed during the sensing mode. These excursions are assumed to be strikes on the probe by large solid particles that do not stick.

Figures 8(a) and (b), respectively, are examples of the unprocessed ice detector data collected during the 6 December 1979 flight, and the same data after the processing procedure had been completed. A flow chart of the computer algorithm of this procedure is included in the Appendix. The various ways in which these processed data sets are analyzed will be described in later sections.

6. ERRORS DUE TO INSTRUMENT LOCATION

In order to determine if measurements of icing by the detector were based on particles representative of flow in the free stream, a theoretical study of the three-dimensional flow about the wing was initiated.[15] Calculations were made of the trajectories of particles embedded in the flow over a range of drop sizes, and an estimate of the probable distortion of the number concentration with respect to free stream concentrations at the probe site was obtained. A full discussion of the computation technique is given by Norment.[16]

A distortion of the number concentration results from the interaction between the trajectory of the droplet due to its momentum and the flow of air as it curves around the leading aircraft surfaces. These effects vary with aircraft speed, dimension of the obstructing surface (in this case the cross-section thickness of the wing and wingtip), and the viscous forces acting on different size drops in the spectrum.

15. Norment, H.G. (1979) Airflow Effects on Riming Measurements by a Wing Tip-Mounted Ice Detector on the MC-130E Research Airplane, AFGL Technical Report 79-0194, AD A077019, 38 pp.

16. Norment, H.G. (1980a) Calculation of Water Drop Trajectories to and About Arbitrary Three-Dimensional Bodies in Potential Airflow, NASA Contractor Report 3291, 82 pp.

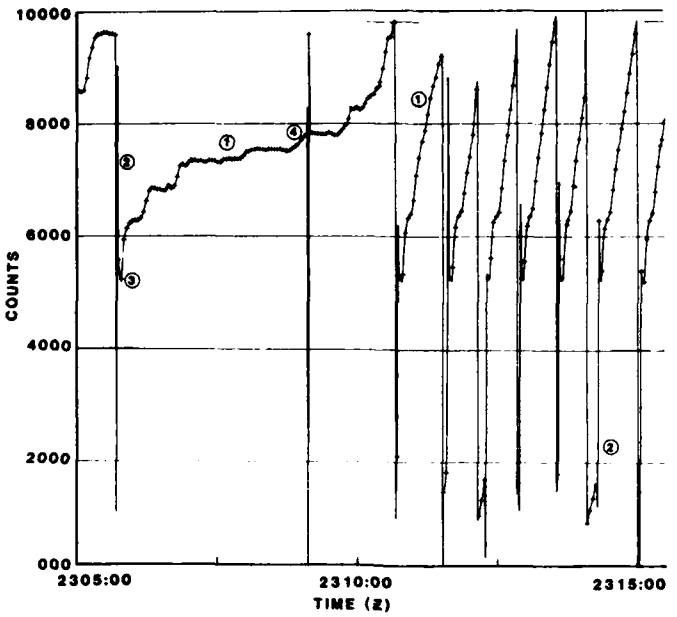

Figure 8. Time Segment of Ice Detector Data. (a) Counts prior to processing. (b) After processing by the algorithm described in text. The circled numbers identify examples of the data characteristics discussed in the text. (1) Sensing mode data. The $\underline{X}$ is the first data point exceeding 6000 counts. (2) Detecting mode. (3) Standby value (+) ≈ 5250 counts. The time of occurrence of this mode for each cycle is indicated. These times are the reference points used to identify the cycles. (4) Examples of random large excursion, removed in processed data by extrapolation technique. (5) Characteristic of sensing data while probe is cooling to ambient condition

Table 3 summarizes the ratio of drop flux to the flux occurring in undisturbed flow for various conditions.[17] The ratio, defined as the concentration factor indicates how well measurements from the probes at the location installed represent free stream conditions. For example, the number density of 20-μm particles expected to be observed at the tip of the probe (10.2 cm) when the aircraft is flying at an angle of attack of 4 degrees is 14.6 percent in excess of the free stream number density. As can be seen, the difference in peak values of the concentration factor at the midpoint and tip positions of the probe indicate that at this location the probe is sensitive to distance from the wing surface. These results suggest that the probe does not quite extend into the free stream with respect to drops in the 30-μm to 80-μm size range.

The distortions in the magnitude of the calculated concentration factors from free stream conditions were not considered excessive, and since those sizes with maximum distortion tend to be larger than the median volume diameter of drops frequently observed during icing conditions (for example, Jeck[18]) it was concluded that the probe's location was acceptable and that information obtained from it could be compared usefully with measurements from the J-W and PMS probes for information on icing rates.

7. INSTRUMENT RESPONSE DURING DATA SAMPLING LEGS

The 12 passes (Figure 1) flown on 6 December 1979, bracket the altitude range of observed icing conditions. These data describe a variety of icing rates and cloud conditions for a range of temperatures. Summary information with data averaged over the length of each pass is shown in Table 4. Pass 1 was flown at an altitude where true temperatures averaged just below freezing. As seen in Table 4, the ice detector cycled during this leg. The usefulness of data from this instrument at these warm temperatures will be discussed later. Pass 8 was apparently made outside a cloud layer, since both the ASSP and J-W indicated negligible (LWC values $< 10^{-2}$ g m^{-3}) liquid water. For passes 7 and 12 the combination of ice accumulation and its evaporation from the probe, occurring when the aircraft broke out of the clouds, caused ice detector cycling to be exceedingly long (> 7 minutes). For these passes, the cycling period exceeded the time the aircraft flew the pass.

17. Norment, H.G. (1980) Calculated Effects on Water Drop Flux Measurement of an Extended Mounting for an Ice Indicator Mounted on the Wing Tip of the MC-130E Research Airplane, Final Report AFGL Contract F197628-80-M-0008, 19 pp.

18. Jeck, R.K. (1980) Icing Characteristics of Low Altitude, Supercooled Layer Clouds, Report No. FAA-RD-80-24, 71 pp.

Table 3. Concentration Factors at Distance of 8.9 and 10.2 cm From Surface of Wing Tip at the Position Probe is Mounted (After H.G. Norment, 1980b)

8.9 cm from the wing tip surface				10.2 cm from the wing tip surface			
Water Drop Diameter (μm)	Angle of Attack			Water Drop Diameter (μm)	Angle of Attack		
	2°	4°	6°		2°	4°	6°
800	1.008	1.005	1.004	800	1.006	1.005	1.004
500	1.017	1.014	1.013	500	1.015	1.013	1.011
300	1.042	1.036	1.019	300	1.037	1.033	1.031
150	1.099	1.086	1.083	150	1.087	1.077	1.074
100	1.169	1.146	1.137	100	1.144	1.127	1.121
80	1.218	1.187	1.171	80	1.181	1.158	1.152
50	1.289	1.259	1.260	50	1.224	1.208	1.209
30	1.224	1.221	1.231	30	1.176	1.183	1.190
20	1.158	...	1.178	20	1.139	1.146	1.154
10	1.095	1.102	1.180	10	1.087	1.085	1.091

Table 4. Summary of Observations During Passes

Pass Number	Start Time (Z)	Stop Time (Z)	Number of Cycles	Mean Period (sec)	SD of Period	Rate R_a (cy/min)	LWC (g/m^3) ASSP	LWC (g/m^3) (Total)	Altitude km	True Temp (C)	Total Temp (C)	DEWP Dep. (C)
1	22:57:10	23:03:08	3	99	77	0.60	0.23	(0.24)	1.79	- 0.8	2.9	< 1.
2	23:03:25	23:10:39	2	205	73	0.29	0.06	(0.07)	2.22	- 1.9	1.8	< 1.
3	23:14:24	23:19:24	7	24	3.5	2.47	0.32	(0.33)	2.82	- 3.6	0.1	< 1.
4	23:23:45	23:28:44	6	29	13.6	2.05	0.23	(0.23)	3.45	- 6.1	- 2.0	< 1.
5	23:29:52	23:38:41	2	250	17	0.24	0.05	(0.05)	4.10	-10.1	- 5.6	< 1.
6	23:41:03	23:44:17	5	22	12.1	2.78	0.32	(0.32)	4.67	-14.6	-10.1	< 1.
7	23:47:54	23:54:42	1	> 400	...	< 0.15	0.01	(0.01)	5.31	-15.7	-10.6	22.
8	00:01:00	00:06:00	0	...	...	...	...	...	5.03	-15.0	...	> 30.0
9	00:08:52	00:14:20	3	77	56.7	0.78	0.13	(0.13)	4.39	-13.3	- 8.7	1.
10	00:18:04	00:24:40	10	22	23.4	2.75	0.28	(0.28)	3.74	- 8.2	- 4.1	< 1.
11	00:28:13	00:31:03	5	19	7.0	3.19	0.31	(0.31)	3.14	- 5.4	- 1.5	< 1.
12	00:31:18	00:42:52	1	> 40[illegible]	...	< 0.15	0.05	(0.06)	2.85	- 5.2	- 1.3	1.4

The total temperature shown in Table 4, when compared with true temperature, indicates the effect of dynamic heating on the measurement of temperature by the Rosemount Temperature Probe. The magnitude of dynamic heating at the icing probe has not been calculated; it is probably small, but not negligible. However, these temperature differences illustrate how dynamic heating can cause a rime icing situation occurring with one given aircraft to become a clear ice, or no icing situation for an aircraft with different aerodynamic characteristics.

Liquid water content values from the ASSP and J-W probes and the response of the ice detector for passes 4, 6, 10 are plotted in Figures 9 (a, b, c). These examples indicate a variety of icing conditions encountered as shown by the character of the ice detector curves. Note the similarity in response of the J-W and ASSP to cloud conditions.

The sensitivity of the ice detector to fluctuations in LWC suggest that usable icing rate relations can be developed in a more detailed manner than simply counting the number of times the probe cycles over a given period.

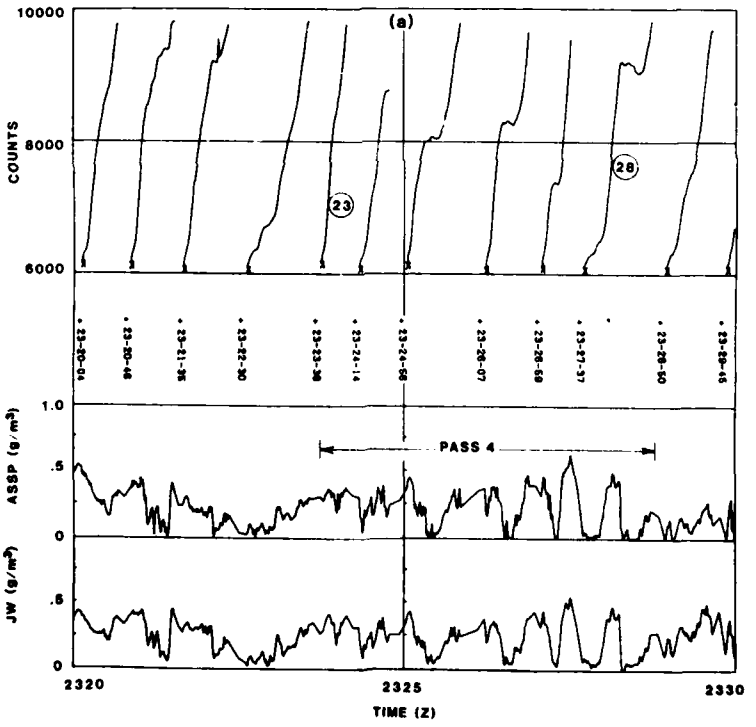

Figure 9a. Liquid Water With Time From ASSP and J-W, Pass 4. Top curves are sensing periods of ice detector cycles. Circled numbers indicate first and last cycle of pass

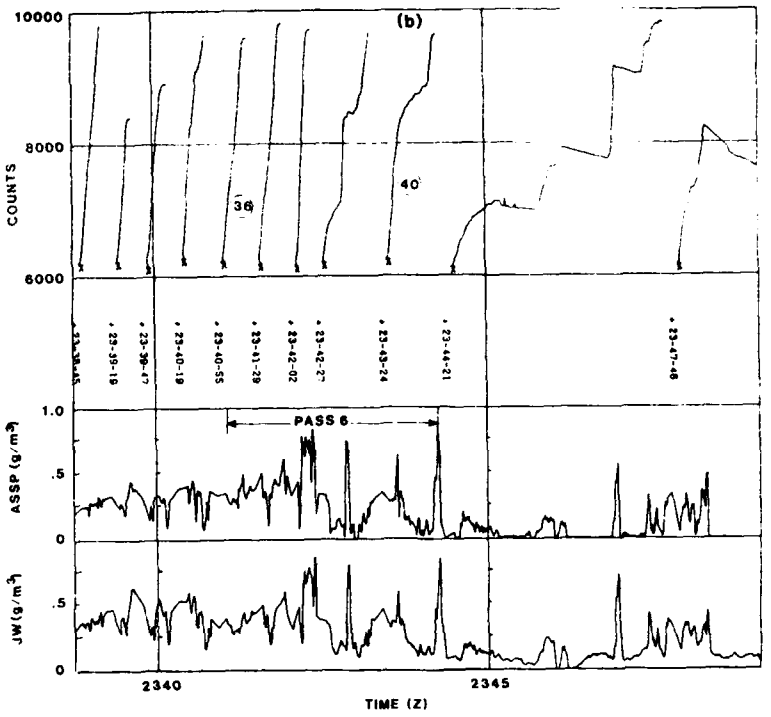

Figure 9b. Liquid Water With Time From ASSP and J-W, Pass 6. Top curves are sensing periods of ice detector cycles. Circled numbers indicate first and last cycle of pass

8. DATA ANALYSIS

In this section, procedures to examine the response of the ice detector to atmospheric aircraft icing conditions are developed. Our purpose is to develop expressions that relate the rate of response of a reference element, that is, the ice detector probe, to the mass of supercooled water available in the atmosphere as measured by the ASSP.

It is important to note that the function of this instrument is to estimate the rate at which ice accretes, and not measure ice accumulation, since the probe cycles to remove ice after a small amount has been accumulated. The manufacturer estimates that the heating cycle is initiated after accumulation of less than 0.05 gram of ice. Therefore, the Ludlam[19] limit, defining the maximum mass of ice that a

19. Ludlum, F.H. (1951) The heat economy of a rimed cylinder, Quart. J. Roy. Meteorol. Soc. 77:663.

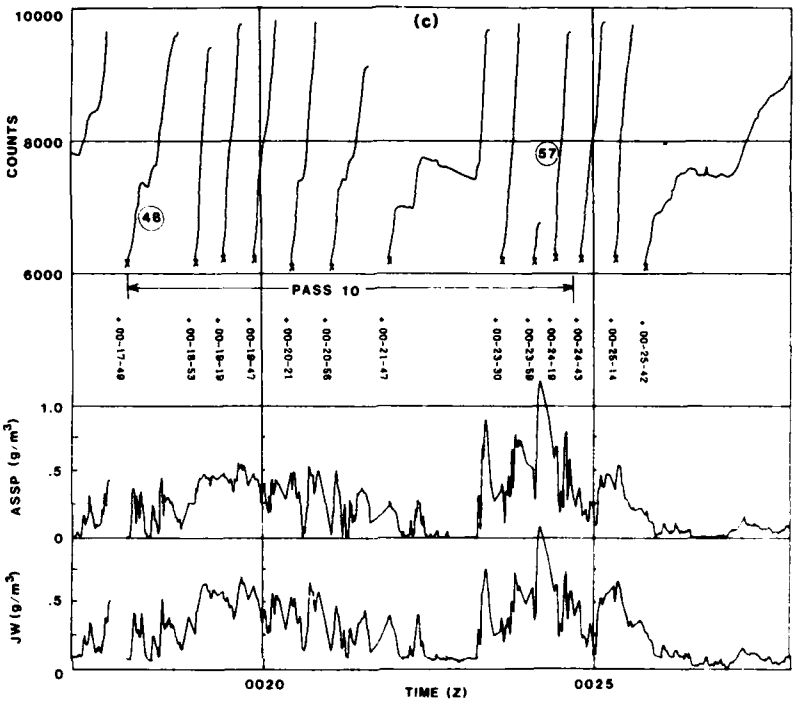

Figure 9c. Liquid Water With Time From ASSP and J-W, Pass 10. Top curves are sensing periods of ice detector cycles. Circled numbers indicate first and last cycle of pass

probe of a given diameter can accumulate at a given temperature and still be proportional to ambient LWC conditions, is not exceeded by the probe and therefore does not constrain the instrument response except at temperatures near freezing.

The manner in which cycling of the probe is examined can be used to define icing rates. Three different approaches to the definition are discussed. Icing rate can be defined as:

1. The number of times the probe cycles during the time of flight on a given leg. Its relation to LWC is given by,

$$R_a = f(\overline{mass})_a \qquad (6)$$

where R_a is expressed as the number of cycles per minute and $\overline{mass}_a$ is the average LWC (g/m^3) encountered during the pass. This average is based only on measurements made while the ice detector is in the sensing mode.

2. The reciprocal of the "useful time period", Δt, that the ice detector is in the sensing mode during each cycle. Its relation to LWC is given by

$$R_b = \Delta t^{-1} = f(\overline{mass})_b \tag{7}$$

where $\overline{mass}_b$ in this case is the average LWC, obtained during the time period Δt of each cycle. A Simpson rule integration is used in the averaging process.

The useful time period, Δt, of the sensing mode is the time segment that data from the detector is compared with measurement from other instruments. The time period, Δt, begins 7 sec after probe counts exceed 6000. This delay is to ensure that the probe has cooled to the ambient temperature. The period ends 3 sec prior to the time at which detector counts exceed 9818. This modification to the original working definition was made to eliminate possible nonrepresentative data points that could result from the extrapolation procedures used to smooth random large excursions when these procedures are applied at the end of the sensing mode.

3. The change in counts per second during each second the probe is in the sensing mode.

Defined in this way, a rate is calculated each second and can be related to the mass obtained each second from the ASSP (=LWC*). In this case

$$R_{c_t} = \Delta \text{Counts}/(3818\Delta t) = f(\text{LWC}^*)_t \tag{8}$$

where 3818 (= 9818-6000) counts per cycle is the maximum value possible in the sensing mode. It is inserted to normalize rate, R_c, so that it has the dimension seconds^{-1}. With this definition of rate, a set of values of R_c is derived for each of the cycles. The number of values obtained in each cycle is equal to $\Delta t+1$.

In order to calculate Δ counts so that the effect of random noise in the data is not exaggerated by the difference equation, a procedure given by Lanczos[20] is used. In this procedure a smoothing polynominal of degree 2k is fitted to the data and an expression for the derivative of the smooth function is developed in order to obtain a rate of change. The general formula for the derivative of a function located at X with k neighbors on each side, and equally spaced is:

$$f'(X) = \sum_{\alpha=-k}^{+k} \alpha f(X+\alpha h)/\left(2 \sum_{\alpha=1}^{k} \alpha^2 h\right) \tag{9}$$

20. Lanczos, C. (1961) Applied Analysis, Prentice-Hall, Inc., 315-324.

where h is the interval between equally spaced observations. In this study,

$$h = 1 \text{ sec} .$$

Calculations of rate, R_c, were made using this derivative formula with k = 1, 2, and 3 neighbors to determine the degree of smoothing necessary to suppress noise without excessively suppressing real variations in the ice detector data.

The formula using k = 2 was found generally satisfactory. The general formula used to calculate R_c was specialized to the difference equation (with time, t replacing X).

$$R_{c_t} = [-2f(t-2) - f(t-1) + f(t+1) + 2f(t+2)]/10 \tag{10}$$

and applied to the counts measured each second of the sensing period of each cycle. The general formula cannot be applied at the first and last two points of each data set. For these points, a noncentered derivative applied to a least-squares second degree fit to the data was used.

The equations for R_c at t=1 and t=2 are:

$$R_{c_{t=1}} = (-21f(1) + 13f(2) + 17f(3) - 9f(4))/20 \tag{11}$$

$$R_{c_{t=2}} = (-11f(1) + 3f(2) + 7f(3) + f(4))/20 . \tag{12}$$

By solving the comparable equation in the reverse direction, one obtains R_c at t_{final} and $t_{final-1}$.

Comparison of these rates with the instantaneous LWC measurements required a similar smoothing of data to filter noise; a five-point smoothing formula given by Lanczos[20] was employed.

$$LWC^*_t = (-3f(t-2) + 12f(t-1) + 17f(t) + 12f(t+1) - 3f(t+2))/35 .$$

The smoothed value for liquid water content, LWC* at the first two points is obtained with the use of the formulas.

$$LWC^*_{t=1} = f(1) + \Delta^3 f(1)/5 + 3\Delta^4 f(1)/35 \tag{13}$$

and

$$LWC^*_{t=2} = f(2) - 2\Delta^3 f(1)/5 - \Delta^4 f(1)/7 , \quad (14)$$

where

$$\Delta^3 f(1) = f(4) - 3f(3) + 3f(2) - f(1)$$

and

$$\Delta^4 f(1) = f(5) - 4f(4) + 6f(3) - 4f(2) + f(1) .$$

Similar smoothing functions at t_{final} and $t_{final-1}$ are obtained by expressing these equations in the reverse direction.

9. EVALUATION OF RATE EQUATIONS

In the following sections the three previously defined rates R_a, R_b, and R_c are evaluated.

Definition 1: R_a

Table 4 lists the value of R_a and the mean LWC for each of the data gathering legs flown. These data are plotted in Figure 10. As can be seen, the cycling frequency and the mean LWC vary similarly for all of the passes, except for pass 1. The mean ambient temperature for this pass is -0.8C. It is probable that the Ludlum[19] limit has been exceeded during the pass and only a fraction of the supercooled water striking the probe has frozen. The rate, R_a, and mean LWC calculated for pass 1 are therefore not expected to be comparable. It is reasonable to exclude these data in the derivation of the function relating R_a and LWC_a.

Applying a linear regression analysis to relate these parameters, one notes that Eq. (6) becomes

$$R_a = -0.1836 + 9.6\,(\overline{LWC})_a . \quad (15)$$

The standard error of estimate for these data is 0.233 and the coefficient of correlation is 0.98. A scatter plot of these data and the regression line with a one-standard error envelope are shown in Figure 11. Also shown in this Figure 11 (circled) is the coordinate of the data point for pass 1 not included in the derivation of Eq. (15).

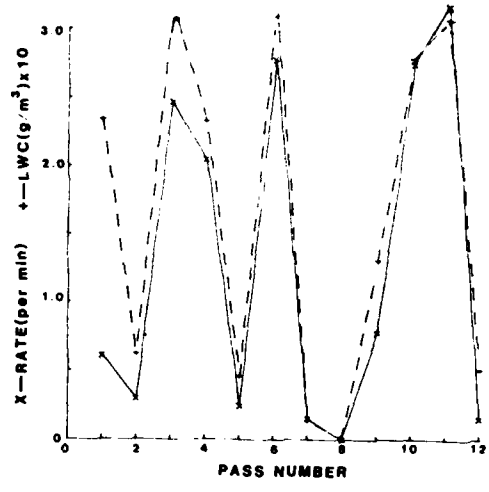

Figure 10. Comparison of Rate, R_a (X, solid line) and $\overline{LWC}_a$ (+, dashed line) for Each Pass

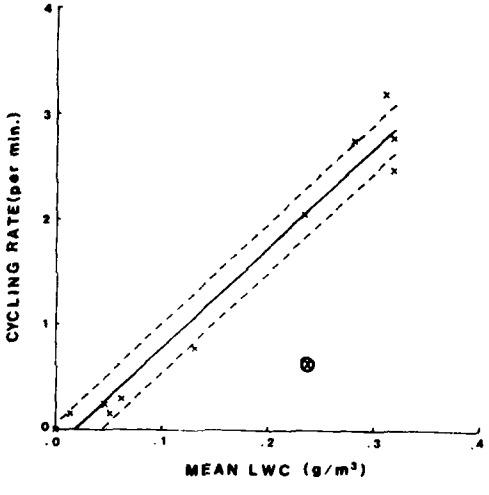

Figure 11. Scatter Plot of Rate R_a vs $\overline{LWC}_a$. Regression line of best fit (solid line) and standard error of estimate lines (dashed) are also shown. Circled value from pass 1 not included in regression calculation.

Applying a typical LWC value of 0.25 g/m^3 for winter stratus to Eq. (15), one obtains a cycling rate of 2.22 ± 0.23 cy/min. This result is based on data collected at the aircraft's true airspeed (TAS), which varied during most of the flight within ± 5 percent of 90 m/sec. Given the assumption that all water impacting on the probe freezes and that the collection efficiency is constant, the rate at which ice collects on a surface is proportional to its TAS. A proportional increase in R_a would be expected. Thus at a TAS of 100 m/sec $R_{a(100)} = 1.11\ R_a$; that is:

$$R_{a(100)} = -0.2038 + 10.7\ (\overline{LWC})_a \ . \qquad (16)$$

It is evident from this calculation that the ice detector becomes a less sensitive instrument for specifying LWC with increasing airspeed.

Definition 2: R_b

As Figure 9 has shown, liquid water content, even over short distances is a highly variable parameter. For this reason, the rates R_b and R_c, which examine the ice detector response on a scale proportional to the liquid water, were defined. The rate, R_b, based on the cycling period, Δt, of the ice detector is evaluated in this section.

During the 12 passes a total of 45 cycling events of the ice detector probe occurred. An additional 23 cycles occurred during the intervals between passes. Data from these events are equally useful in characterizing icing conditions. Information on each of the 68 events are summarized in Table 5. The mean liquid water ($\overline{LWC}$) tabulated is the value averaged over the period Δt. The median volume diameter, MVD, is obtained using $\overline{LWC}$ and the mean droplet spectra.

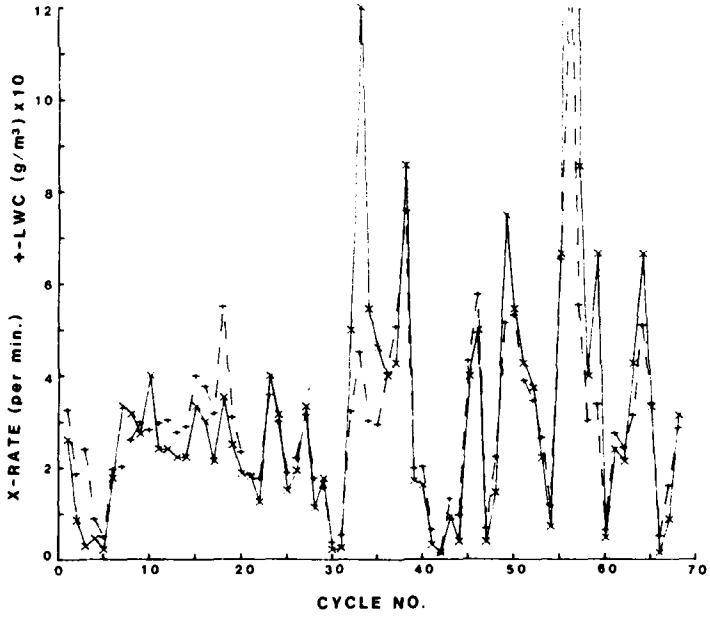

Figure 12. Comparison of Rate, R_b (X, solid line) and $\overline{LWC}_b$ (+, dashed line) for Each of 68 Cycles

The rate R_b and $\overline{LWC}_b$ are plotted in Figure 12 for each of the 68 cycling events that occurred during this icing studies mission. This figure is analogous in its form to Figure 10 and illustrates the variability of LWC in winter stratiform clouds. The LWC and rate R_b (shown in Figure 12 with dimension, min^{-1}) are seen to vary similarly. It is expected then, that these data expressed in the form derived here, can be used to form a relation between the response of the probe and the mass of supercooled liquid water.

Table 5. Cloud Characteristics Occurring With Each Cycle

Cycle Number	Pass Number	Period Δt sec	$\overline{LWC}$ g/m^3	MVD μ m	Temp °C
1	1	23	0.326	14	- 2.0
2	1	70	0.186	12	- 0.9
3	1	205	0.240	16	- 0.6
4	2	132	0.088	11	- 1.5
5	2	276	0.049	9	- 2.0
6		34	0.196	19	- 2.7
7		18	0.202	11	- 3.0
8		19	0.259	13	- 2.8
9		22	0.297	13	- 4.1
10		15	0.281	13	- 4.0
11	3	25	0.296	17	- 3.7
12	3	25	0.303	16	- 3.8
13	3	27	0.276	16	- 3.6
14	3	27	0.289	20	- 3.4
15	3	18	0.399	20	- 3.7
16	3	20	0.377	17	- 3.6
17	3	28	0.318	16	- 3.4
18		17	0.550	20	- 3.6
19		24	0.310	19	- 4.2
20		32	0.234	16	- 5.5
21		33	0.184	11	- 6.1
22		48	0.176	11	- 6.0
23	4	15	0.358	14	- 6.3
24	4	19	0.300	15	- 6.2
25	4	40	0.188	15	- 5.9
26	4	31	0.220	15	- 6.1
27	4	18	0.315	16	- 6.2
28	4	53	0.177	16	- 6.2
29		34	0.157	12	- 7.6
30	5	267	0.038	16	-10.0
31	5	233	0.053	14	-10.1
32		12	0.323	13	-13.0
33		5	0.452	14	-14.2
34		11	0.302	13	-14.7
35		13	0.295	14	-14.6
36	6	15	0.407	14	-14.2
37	6	14	0.507	16	-14.3
38	6	7	0.758	18	-14.3

Table 5. Cloud Characteristics Occurring With Each Cycle (Cont)

Cycle Number	Pass Number	Period Δt sec	$\overline{LWC}$ g/m^3	MVD μ m	Temp °C
39	6	35	0.198	15	-15.0
40	6	37	0.202	16	-14.7
41		184	0.065	13	-15.4
42	7	> 399	0.014	16	-15.7
43	9	64	0.132	16	-13.2
44	9	152	0.097	18	-13.3
45	9	15	0.433	17	-13.4
46		12	0.577	17	-12.5
47		152	0.068	15	- 9.0
48	10	41	0.223	14	- 8.6
49	10	8	0.515	15	- 8.6
50	10	11	0.532	16	- 8.5
51	10	14	0.390	16	- 8.5
52	10	16	0.346	17	- 8.4
53	10	27	0.265	16	- 8.2
54	10	84	0.118	18	- 7.9
55	10	9	0.654	22	- 8.1
56	10	1	1.332	24	- 8.2
57	10	7	0.555	23	- 8.0
58		15	0.302	20	- 6.6
59		9	0.338	18	- 5.5
60		126	0.064	9	- 4.9
61	11	25	0.275	11	- 5.2
62	11	28	0.244	11	- 5.1
63	11	14	0.315	12	- 5.3
64	11	9	0.511	16	- 5.5
65	11	18	0.341	17	- 6.0
66	12	> 399	0.051	29	- 5.2
67		68	0.161	11	- 3.0
68		19	0.287	12	- 3.3

In order to test whether ambient temperature was a factor in the response of the ice detector probe, the data were grouped in four classes defined by the temperature ranges:

1. 0C to -4C (18)
2. -4.1 to -8 (22)
3. -8.1 to -12 (10)
4. -12.1 to -16 (14)

Scatter diagrams of log (Δt^{-1}) vs $\overline{LWC}_b$ were plotted for the data included in each of the four groups and linear regression relations were calculated [Figure 13 (a, b, c, d)]. The numbers in parentheses (above) indicate the number of data pairs used in each group.

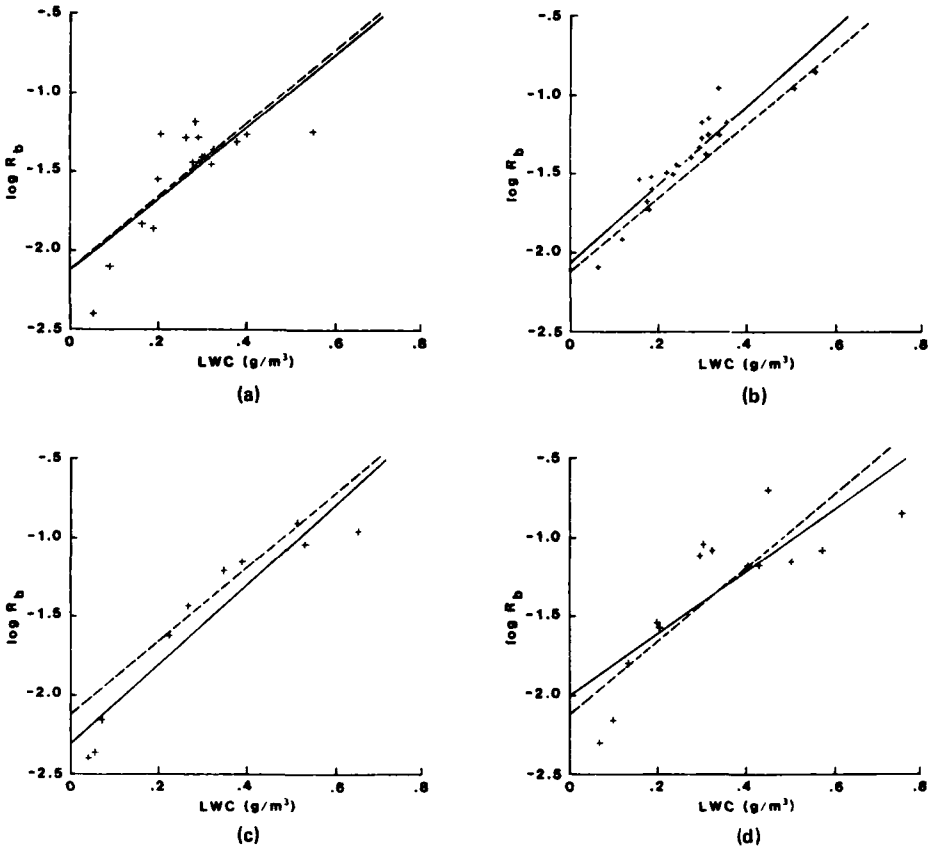

Figure 13. Scatter Plot of Log R_b vs $\overline{LWC}_b$ and Regression Line of Best Fit (solid line). Four groups plotted are for different temperature regimes defined in text. Dashed line is mean regression line of best fit [Eq. (18)]

Data from 4 of the 68 cycles were excluded in plotting these data and in calculating the regression line. The excluded data are from cycle 42 and 66 in which the sensing period exceeded 7 min; cycle 3 in which the mean true temperature was near 0°C, and cycle 56. Data from this latter cycle were excluded since the probe rate of cycling was too rapid to obtain a usable measure of the period, Δt. The greatest amount of supercooled water (LWC = 1.33 g m^{-3}) during the flight was observed at the time of this cycle. Mason[21] quotes maximum LWC values observed in stratocumulus layers to be 1.30 g m^{-3} and typical values ranging from 0.07 to 0.83 g m^{-3}. The data collected on this flight are therefore considered a representative sample.

21. Mason, B. J. (1971) The Physics of Clou Clarendon Press, 115-121.

The algorithm defining the sensing period breaks down when the number of seconds that elapse while the sensing mode is between 6000 and 9818 counts is less than 12. The algorithm is modified for this case so that when < 12 but > 7 sec sensing records remain, the first 6 and one last point (instead of three) are deleted. When only 7 sec of the sensing record remain, the first 5 are deleted. The remaining 2 points give the nominal $\Delta t = 1$ second. This latter situation characterized cycle 56.

The regression equations and their standard error of estimate, SE, relating $R_b (= \Delta t^{-1})$ and $\overline{mass}_b$ are, for each of the temperature groups:

$$\begin{aligned}
\text{Log } R_{b(1)} &= -2.1050 + 2.2633\ (\overline{LWC})_b \\
SE &= 0.20 \\
\\
\text{Log } R_{b(2)} &= -2.0761 + 2.4952\ (\overline{LWC})_b \\
SE &= 0.11 \\
\\
\text{Log } R_{b(3)} &= -2.3075 + 2.5450\ (\overline{LWC})_b \\
SE &= 0.18 \\
\\
\text{Log } R_{b(4)} &= -2.0009 + 1.9582\ (\overline{LWC})_b \\
SE &= 0.26
\end{aligned} \qquad (17)$$

The dashed line in Figure 13 (a, b, c, d) is the mean regression line derived from identical data pairs calculated from each of the 4 regression equations. This procedure was used to give equal weight to each of the 4 groups of data in deriving the mean regression equation. The equation derived is:

$$\text{Log } R_b = -2.1224 + 2.3154\ (\overline{LWC})_b\ . \qquad (18)$$

Comparison of Eq. (18) with Eq. (17) suggests that the 4 curves, each derived for different temperature ranges, are not significantly different. The response of the ice detector, except for temperature close to freezing, is apparently independent of temperature. This result is not surprising, since the probe with a diameter of 0.635 cm and cycling after the accumulation of small amounts of ice, never accumulates sufficient mass, at the airspeed flown, to exceed the Ludlum[19] limit. The Ludlum limit for the ice detector probe flown at 100 m/sec is approximately 0.3 g m^{-3} at -10°C.

Equation (18), evaluated for a range of LWC values, is tabulated in Table 6. These data show that, with the use of the analysis procedure defining R_b, the ice detector probe can reasonably estimate supercooled liquid water content over the

range normally expected to be observed in winter stratiform clouds. As can be seen, the sensing period becomes very short when the LWC reaches 0.8 g m^{-3}. The probe was unable to cycle sufficiently fast to permit the foregoing analysis when the extreme value of LWC (1.33 g m^{-3}) was observed. It would be expected then, that the ice detector in its current configuration would be overwhelmed in a cumulus congestus environment where values of supercooled water well in excess of 2.0 g m^{-3} have been observed.[21]

Table 6. Evaluation of Eq. (18) Relating Icing Rate, R_b to $\overline{LWC}_b$

LWC (g m^3)	R_b (sec^{-1})	Period (sec)
0.1	0.0129	77.8
0.2	0.0219	45.6
0.4	0.636	15.7
0.6	0.1849	5.4
0.8	0.5369	1.8

Definition 3: R_c

With this form of icing rate, the derived instantaneous values of R_c and LWC* calculated each second during the active sensing period of a cycle are compared. Six examples (two each from passes 4, 6, and 10) considered representative of this analysis are plotted in Figure 14. It is evident from these data that the instantaneous rate of ice accretion is proportional to the LWC obtained from the ASSP probe. The response with time of these instruments (and the J-W) appear similar, although not identical. The figures give experimental evidence to support Norment's[16] conclusion based on a mathematical study—that the ice detector probe is sufficiently well located on the aircraft to be in the free airstream with respect to the droplet spectra encountered.

Scatter plots of R_c vs LWC* that illustrate quantitatively the relation of the two parameters are displayed in Figure 15 for each of the six cycles of Figure 14. Also plotted are the derived linear regression curves with their one-standard error envelopes.

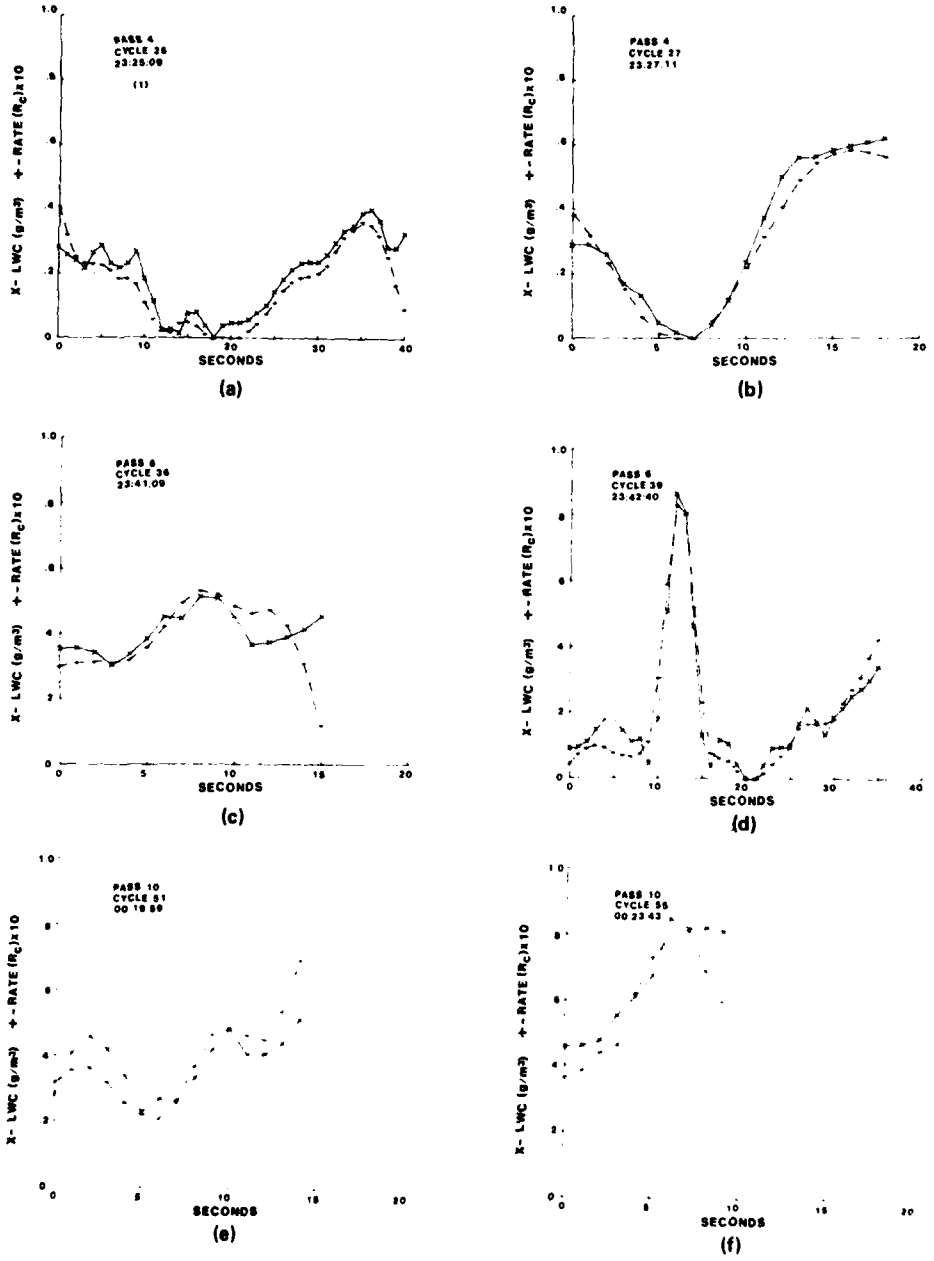

Figure 14. Sample Comparisons of Rate, R_c (+, dashed line) and LWC* (X, solid line) for Cycle Number and Time Indicated

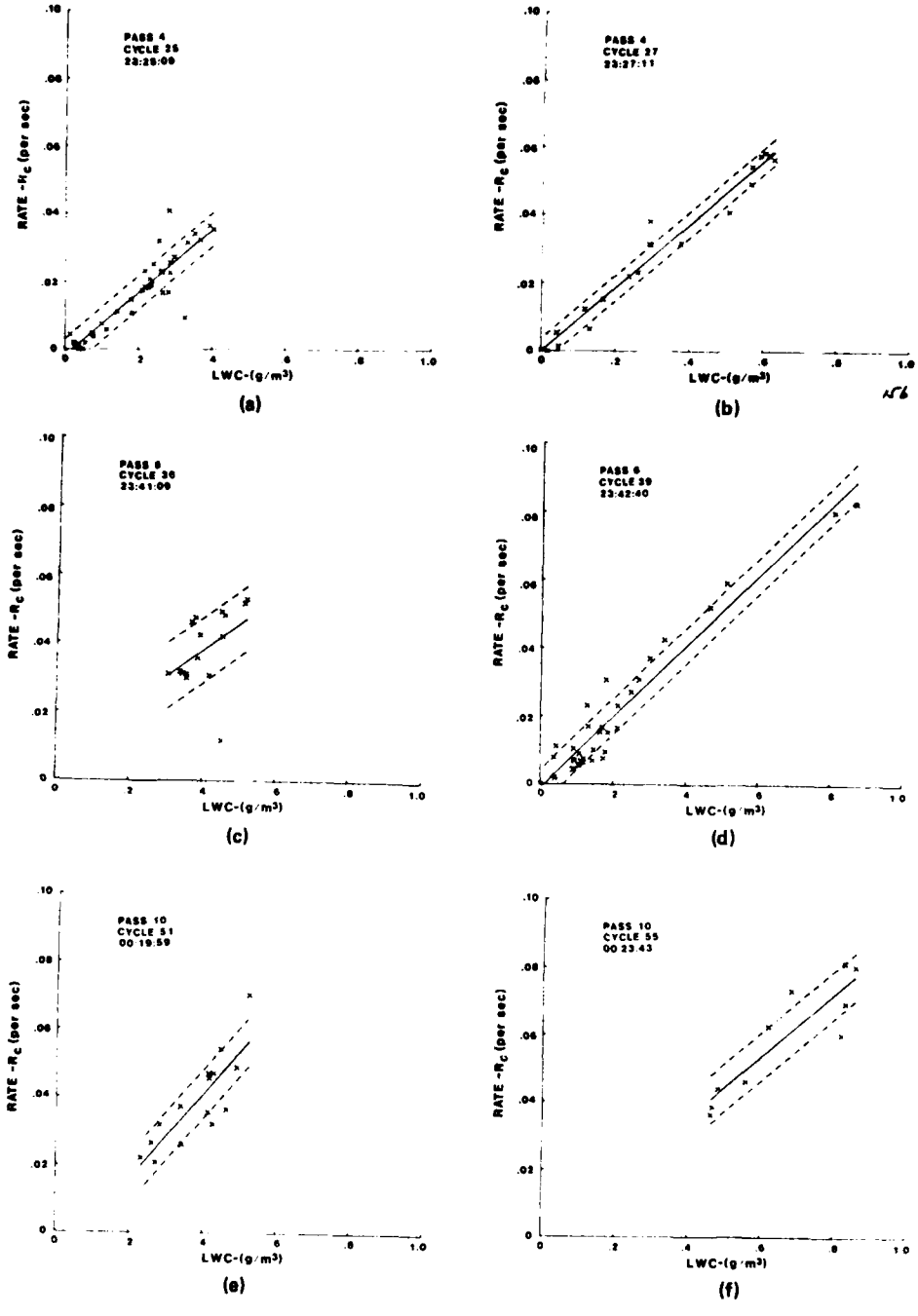

Figure 15. Scatter Plot of Rate, R_C, vs LWC* and Regression Line of Best Fit for Each Cycle Shown in Figure 14. Dashed lines indicate standard error of estimate

Possible lags in the data introduced by the smoothing procedures have not been considered. It is also not known if aircraft orientation during turns and climbs affects instrument response. Distortions in the derived data for all these reasons tend to reduce the correlation between R_c and LWC*, particularly for these conditions: where the LWC is changing rapidly, where the icing cycle is very short, and for situations in which LWC amounts are very small. In addition, the correlation would be reduced by the presence of frozen particles, measured by the ASSP, but not collected by the ice detector. Nevertheless, with the varied conditions observed during the flight, a great majority of the icing cycles indicate high positive correlation between R_c and LWC*. This result is summarized in Figure 16. Note that the same 4 cycles excluded from the derivative of Eq. (18) were not used.

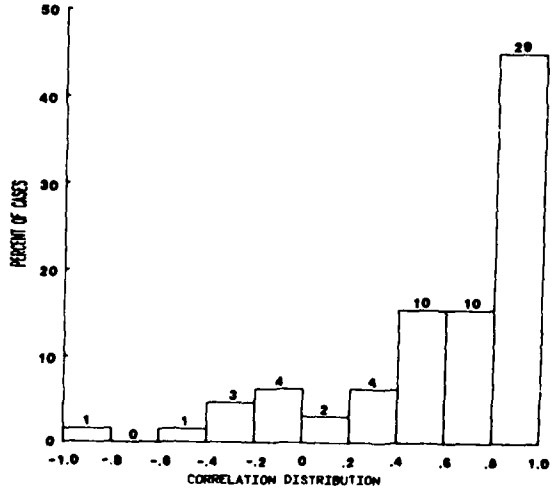

Figure 16. Percentage Distribution of Correlations Between Rate, R_c, and LWC* for 64 Icing Events. Number of cases for each correlation class is indicated above bars

An examination of the characteristics of the icing cycles that comprise the distribution in Figure 16 shows that of the 15 cycles with poor correlations, that is, those between + 0.4 and -1.0, five (33 percent had icing periods ≤ 12 seconds.

Of the remaining 10 cycles in the group, 8 occurred in the lowest altitudes where the ambient temperature and the aircraft's true airspeed resulted in total temperatures that were approximately 0°C and warmer. In addition, this is the region where snow particles were observed.

It is reasonable to conclude, therefore, that in clouds where the rate of ice accretion is light, the response of the ice detector is sufficiently sensitive; the data can be used for estimating the detailed distribution of LWC from supercooled droplets.

10. CONCLUSIONS

These data, based on observations of 6 December 1979, are considered representative of the range of meteorological conditions that would be encountered in winter stratiform cloud systems. These data are not considered representative of meteorological conditions causing severe icing.

On this day, some small snow was observed at the lower pass levels. These snow particles were counted by the PMS cloud probe. The liquid water content derived from these data was found to be a small fraction of the liquid water obtained from the ASSP. Cloud probe data were therefore not included in the analysis.

The liquid water content measurements ranged typically up to 0.8 g m^{-3} with a few values exceeding 1.0 g m^{-3} for a total time of approximately 10 sec of the flight. Graphs of the frequency of occurrence of liquid water mass amounts and median volume diameters during 65 cycling events are shown in Figures 17 and 18, respectively. The bar graphs are based on the average LWC and drop size spectra calculated from the measurements made during the time interval defined by the sensing period of each of the cycles. Three of the 68 cycles occurring during the flight were not included in these distributions: cycles 42 and 66, since icing rates were negligible; and cycle 3, since some temperatures were above freezing, although its mean temperature was approximately 0°C. The cycle in which the LWC was 1.3 g m^{-3} was included, although not shown in Figure 17. The distributions are therefore representative of conditions when icing was occurring. The total flight duration was 2 hours and 27 minutes. Liquid water contents less than 0.025 g m^{-3} as measured each second by the ASSP occurred 38 percent of this time. By these criteria, the aircraft encountered icing conditions during 62 percent of its flight.

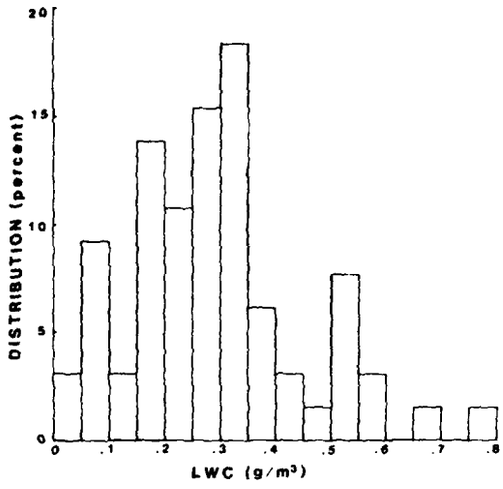

Figure 17. Distribution of LWC_b From 65 Icing Cycles

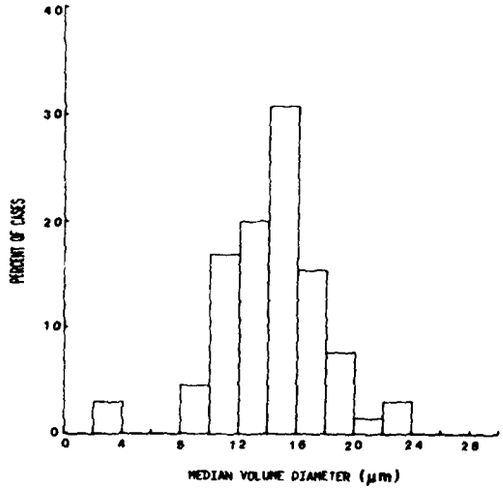

Figure 18. Distribution of Average Median Volume Diameter During Each of 65 Icing Cycles

In this report, a procedure has been developed for adjustment of the drift in measurements of liquid water by the J-W instrument. The ASSP channel size

specification was adjusted by a fraction of the amount recommended by the manufacturer based on the following assumption: That the response of the instrument had decayed linearly between the time it had been used for this study and the time calibrated. These results suggest that a reasonably good estimate of supercooled liquid water occurring on this day was obtained by both instruments. Since the J-W instrument confirmed that liquid water was measured by the ASSP, the latter instrument was chosen as the reference instrument. The ASSP has the additional advantage of measuring number concentration of the droplet spectra.

The Rosemount Ice Detector, recently installed on the Cloud Physics MC-130E research aircraft, had previously been shown, by analysis of the circulation about the wing,[17] to be in the free stream with respect to drop sizes most frequently encountered in icing situations. In this study, comparison of detector response with that of the LWC probes indicates a high correlation. This result substantiated that the choice of location at the wingtip was satisfactory.

A computer algorithm was developed to identify the logical steps in the operation of the Rosemount Ice Detector and extract usable information. The processed data were analyzed in three ways to characterize the cycling rate, R, of the Ice Detector. Each rate; R_a, R_b, and R_c, respectively, defined the instrument cycling on a more detailed scale. Comparisons were then made with an appropriate measurement of LWC obtained from the ASSP.

The rate R_a, defined as the number of cycles of the ice detector occurred during the time of a pass performance, was compared with the mean liquid water content over the length of the pass. The analysis is appropriate for obtaining instrument response and conditions over long flight legs, and during heavy icing conditions when the probe is cycling rapidly; R_a and LWC_a were found to be highly correlated and the regression Eq. (15) was derived.

The rate, R_b, defined as the inverse of the time elapsed during the sensing period was compared with the mean liquid water content occurring during each period. This analysis is appropriate for characterizing the variability of liquid water in stratiform clouds and the response of the ice detector in varying conditions. Sixty-eight cycles of the probe occurring during the course of the flight were examined. As a result, it was estimated that the ice detector is overwhelmed when the LWC exceeds 0.8 g m^{-3}. The instrument is therefore appropriate for most wintertime stratiform conditions, but probably inadequate, except as an indicator of icing occurrence, in convective clouds where values of LWC in excess of 2.0 g m^{-3} are often observed. The regression equation relating R_b and $\overline{LWC}_b$ is given by Eq. (18).

The instantaneous rate, R_c, comparing the slope of the sensing period of the ice detector with a filtered liquid water content value, LWC*, each second, has

been developed to test the sensitivity of the probes to rapid fluctuations in liquid water. It has been found that during icing conditions where the mean LWC during a cycle ranged up to ~ 0.3 g m^{-3}, the rates obtained were highly correlated with LWC. Thus, the ice detector is a sensitive instrument for estimating LWC, as well as fluctuations under these conditions. The observed range of liquid water, however, is sufficient reason for not developing a general relation from this type of analysis.

The J-W liquid water content meter, originally developed to measure icing intensity, and the PMS probes are the preferred instruments for measuring liquid water. The ice detector's initial function is to determine whether or not measurements are in supercooled liquid water clouds. The cycling of this probe has been shown to be a quantitative measure of liquid water within the limits described in this report.

References

1. Advisory Group for Aerospace Research and Development (AGARD) Report No. 127, Aircraft Icing, 1977, North Atlantic Treaty Organization.
2. Frost, W., and Camp, D. W. (1978) Proceedings: Second Annual Workshop on Meteorological and Environmental Inputs to Aviation Systems, NASA Conference Publication 2057, 259 pp.
3. Blaha, B. J. (1979) Aircraft Icing, NASA Conference Publication 2086, 147 pp.
4. Perkins, P. J. (1959) Summary of Statistical Icing Clouds Data Measured Over the United States and North Atlantic, Pacific and Arctic Oceans During Routine Aircraft Operations, NASA Memo 1-19-59E.
5. Lewis, W. (1951) Meteorological Aspects of Aircraft Icing, Compendium of Meteorology, Am. Meteorol. Soc., 1197-1203.
6. Jackson, G. C. (1979) AEROICE: A Computer Program to Evaluate the Aerodynamic Penalties Due to Icing, Air Force Flight Dynamics Laboratory TM-79-91-WE, 22 pp.
7. Hankey, W. L., and Kirchner, R. (1979) Ice Accretion of Wing Leading Edges. Air Force Flight Dynamics Laboratory TM-79-85-FXM, 32 pp.
8. Neel, C. B., J., and Steinmetz, C. P. (1952) The Calculated and Measured Performance Characteristics of a Heated-Wire Liquid-water Content Meter for Measuring Icing Severity, Tech. Notes Nat. Adv. Comm. Aero, Wash., No. 2615.
9. Neel, C. B. (1955) A Heated-wire, Liquid Water-content Instrument and Results of Initial Flight Tests in Icing Conditions, Res. Memo., Nat. Adv. Comm. Aero., Wash., No. A54123, 33 pp.
10. Owens, G. V. (1957) Wind Tunnel Calibrations of Three Instruments Designed for Measurement of Liquid Water Content of Clouds, Cloud Physics Lab., University of Chicago, Tech. Note No. 10, 15 pp.
11. Spyers-Duran, P. (1968) Comparative measurements of cloud liquid water using heated wire and cloud replicating devices, J. Appl. Meteorol, 7:674-678.

12. Knollenberg, R.G. (1972) Comparative liquid water content measurements of conventional instruments with an optical array spectrometer, J. Appl. Meteorol. 11:501-508.

13. Pinnick, R.G., and Auverman, H.J. (1979) Response characteristics of Knollenberg light-scattering aerosol counters, J. Aerosol Sci. 10:55-74.

14. Walsh, P.A. (1977) Cloud Droplet Measurements in Wintertime Clouds, M.S. Thesis, Univ. of Wyoming.

15. Norment, H.G. (1979) Airflow Effects on Riming Measurements by a Wing Tip-Mounted Ice Detector on the MC-130E Research Airplane, AFGL Technical Report 79-0194, AD A077019, 38 pp.

16. Norment, H.G. (1980a) Calculation of Water Drop Trajectories to and About Arbitrary Three-Dimensional Bodies in Potential Airflow, NASA Contractor Report 3291, 82 pp.

17. Norment, H.G. (1980b) Calculated Effects on Water Drop Flux Measurement of an Extended Mounting for an Ice Indicator Mounted on the Wing Tip of the MC-130E Research Airplane, Final Report AFGL Contract F197628-80-M-0008, 19 pp.

18. Jeck, R.K. (1980) Icing Characteristics of Low Altitude, Supercooled Layer Clouds, Report No. FAA-RD-80-24, 71 pp.

19. Ludlum, F.H. (1951) The heat economy of a rimed cylinder, Quart. J. Roy. Meteorol. Soc. 77:663.

20. Lanczos, C. (1961) Applied Analysis, Prentice-Hall, Inc., 315-324.

21. Mason, B.J. (1971) The Physics of Clouds, Clarendon Press, 115-121.

Appendix A

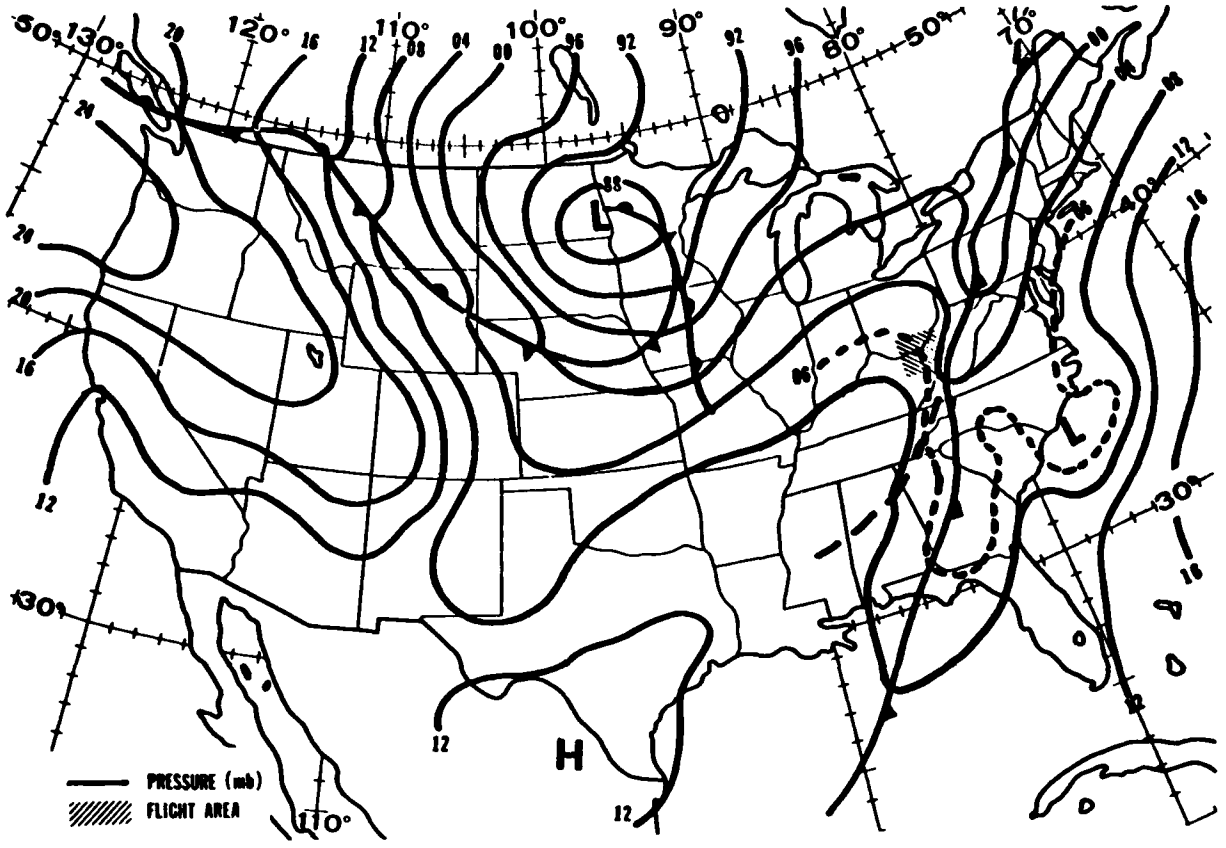

Figure A1. Surface Pressure Chart for 0000Z 7 December 1979 Showing Position of Cold Front and Flight Area (shaded)

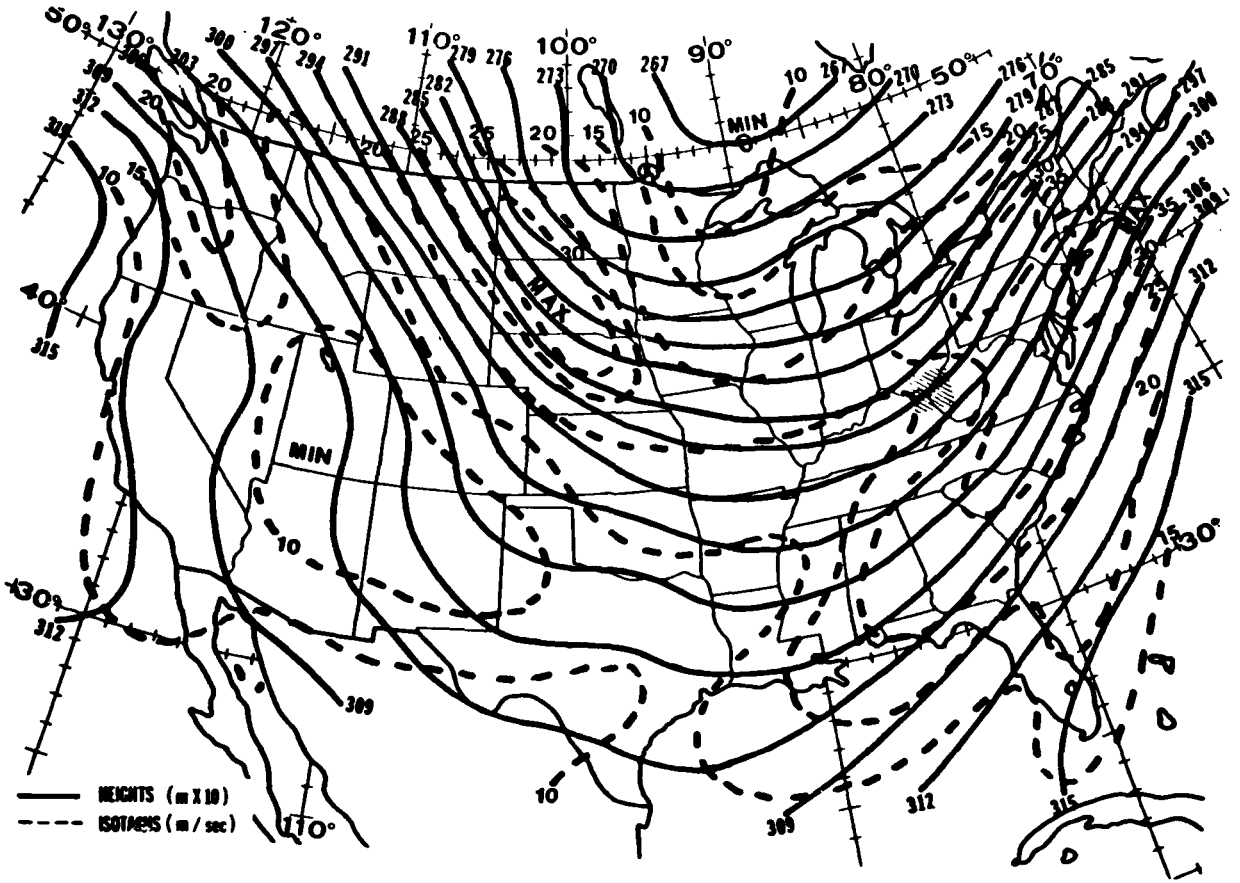

Figure A2. 700-mb Chart for 0000Z 7 December 1979. Flight area is shaded

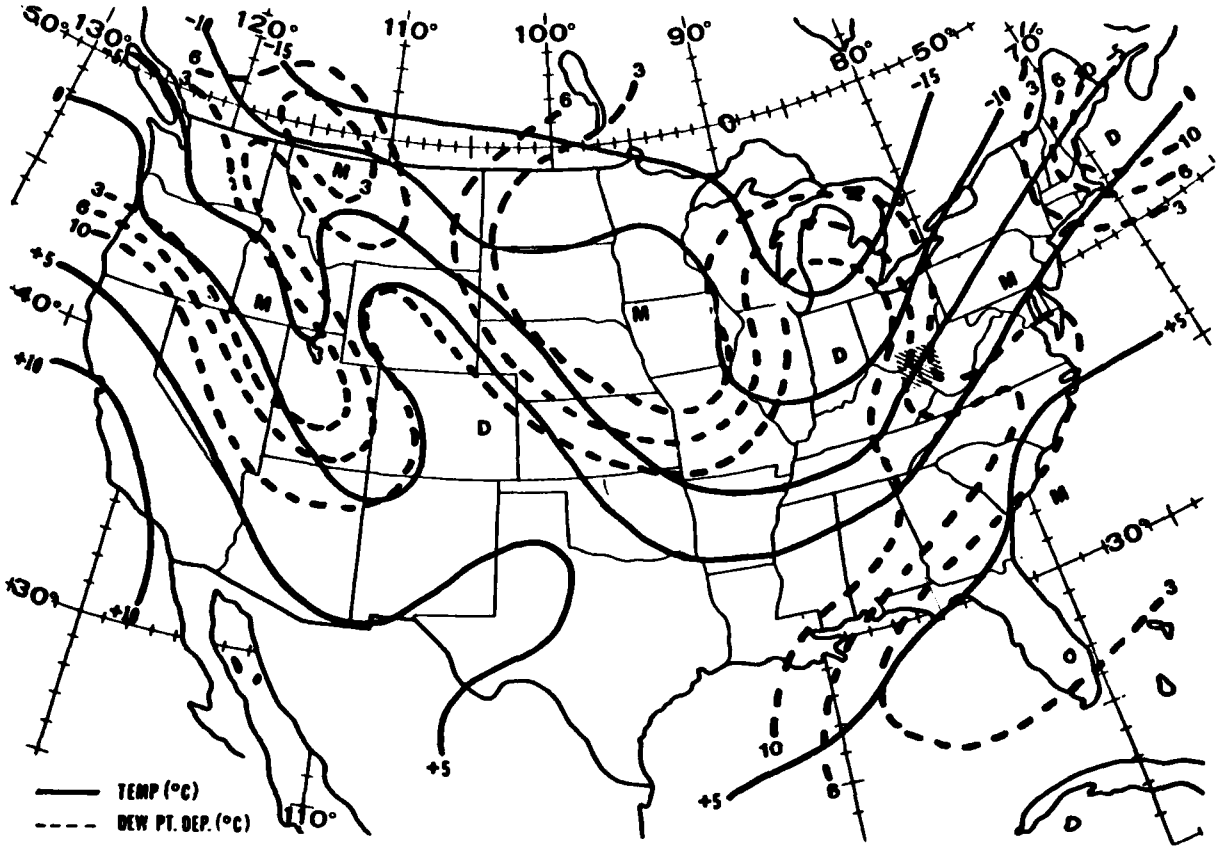

Figure A3. 700-mb Temperature and Dew Point Depression Isolines for 0000Z 7 December 1979

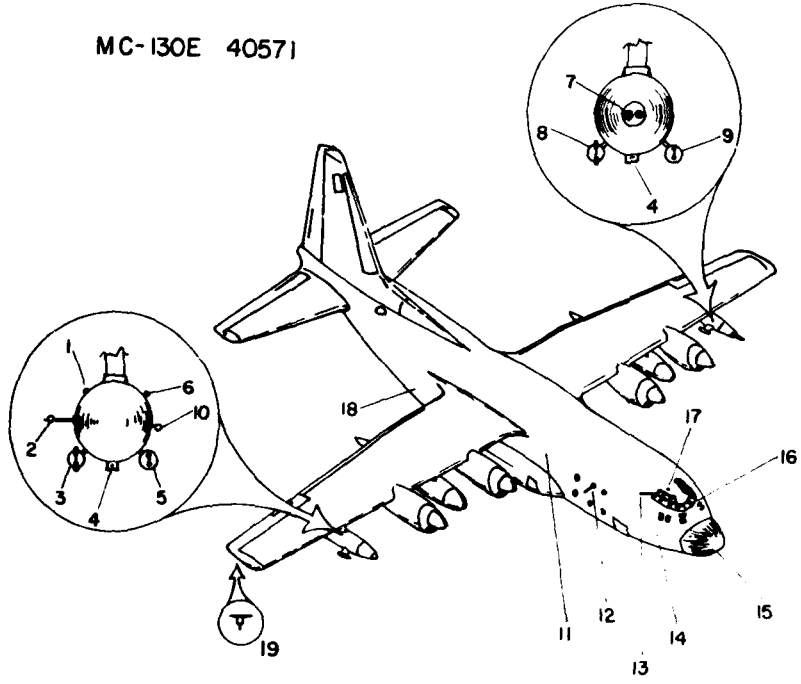

Figure A4. Schematic Figure of MC 130E Aircraft, Serial Number 40571. The cloud physics instrumentation and location on the aircraft are shown

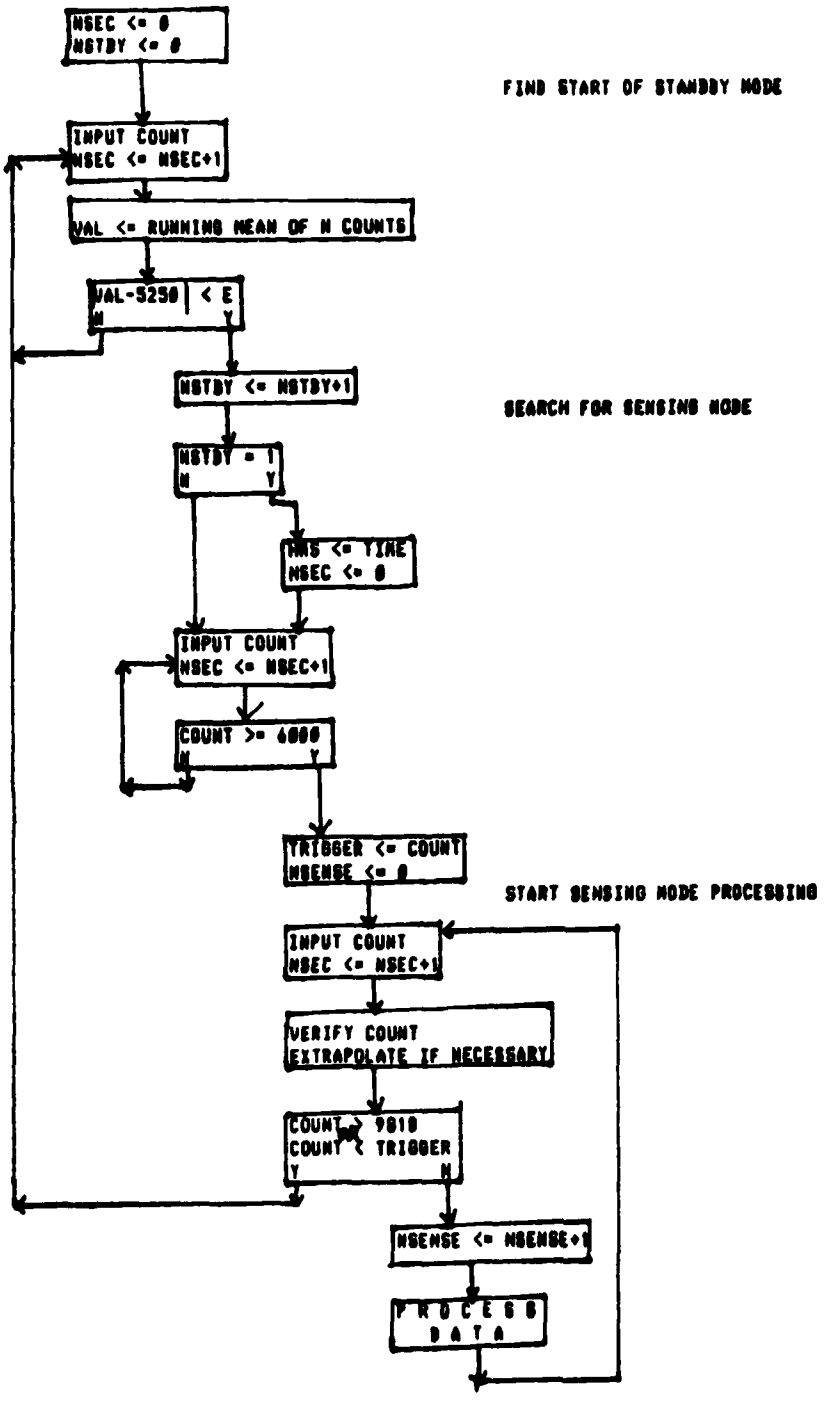

Figure A5. Flow Chart of Algorithm for Processing Ice Detector Data

E	TOLERANCE LEVEL AROUND 5250 (START OF STANDBY MODE)
NSTBY	NUMBER OF OCCURRENCES OF STANDBY MODE
N	AVERAGING INTERVAL OF THE RUNNING MEAN
VAL	RESULT OF THE RUNNING MEAN ON N DATA POINTS
HMS	HOURS, MINUTES, AND SECONDS OF THE FIRST ACCEPTED STANDBY MODE
NSEC	NUMBER OF ELAPSED SECONDS RELATIVE TO HMS
COUNT	VCO VALUE OF THE ICING METER
TRIGGER	VALUE AT WHICH CURRENT SENSING MODE WAS INITIATED (COUNT>6000)
NSENSE	LENGTH OF TIME IN CURRENT SENSING MODE


DATE
ILME
8